Spectroscopy in Ce^{3+}:Y_2SiO_5
A preliminary investigation for a single ion readout scheme for quantum computation with rare-earth ion doped crystals.

Master's thesis

by

Julio E. Hernández

Lund Reports on Atomic Physics, LRAP-356
Lund, March 2006

Contents

Introduction

The computational resources used for science and research in particular and in daily life in general are approaching an unavoidable limit. This limit is set by the relevance of a quantum mechanical description of the system used for the computation and determined by the presence or absence of disturbing quantum effects. This happens because the ideas behind the development of computational hardware in the last decades has relied on the rules of classical physics. Following the miniaturization undergone by the components used for data processing the quantum effects might soon not be negligible and the classical description could become inaccurate.

The field of quantum computation aims to offer solutions on this issue by creating and using a purely quantum system to make computations. Theoretical and experimental results have proven that constructing a computational system described by quantum mechanical laws is feasible. Additionally, such device might indeed enhance the computational power required for at least some selected problems outperforming the current technologies. The general ideas and principles that such technology should follow in the first stage are well settled and backed by research on different areas in physics and information science. On the other hand, efforts towards building the actual devices capable of handling the quantum systems are still in a development stage. Among the main issues to be solved is to find out an appropriate physical system in which to carry out the computations and storing information. The physical processes required to manipulate the quantum system and drive the desired computational algorithms also still need to be found.

One of the approaches currently being investigated to provide the physical system as well as the set of tools necessary to perform the logic operations is that referred as the rare-earth ions doped crystals for quantum computing scheme. There are promising results that make this approach interesting and challenging to work with. However, there are still relevant details that must be worked out. One of these necessary parts is to find a way to make the process used to extract the total or partial results of the computations more efficient. A single-ion readout scheme has been proposed as a way to increase the efficiency of this process. Given the nature of the components proposed for computation some preliminary investigations are needed before trying to implement the scheme. This thesis is an effort to shine some light on some of the previous requirements.

The personal motivation to get involved in this thesis project was to learn more about the overall state of quantum computation and quantum information as an emerging field of

science. I was also very interested in doing experimental work to reinforce the knowledge -or the absence of it- from the theoretical courses in which everything works perfectly once the math is solved. Needless to say that theory and experiment match only after long hours of work and many liters of coffee when you (that's me) are not an expert. My hope is that the experience remains somewhere where I can use it later.

The work done for this project is divided in five chapters with the following contents. In chapter 1 a general review and the basic components of quantum computing are presented. Chapter 2 explains the main features of rare-earth ions and the interesting features appearing when they are doped in crystals as well as the scheme for using them in quantum computing. The main purpose of this thesis is explained in chapter 3 where the method to enhance the readout using an intermediate ion in the single-ion readout scheme is described. In chapter 4 is given a description of the experiments implemented to explore the feasibility of the scheme addressing the fluorescence lifetime as well as absorption and emission spectra using the proposed readout rare-earth ion, cerium (Ce). The results of the experiments are reported and discussed in chapter 5 and conclusions and future perspectives are presented in chapter 6.

Chapter 1

Quantum Computing

Performance of current classical computing faces several challenges to meet the user-imposed demands in the near future. Among the main ones are those referring to the constant miniaturization of processors and components and those related to the always increasing need for higher computational power. Both represent theoretical and technological difficulties and different approaches can be undertaken to explore new ways to solve them. It seems that the only way to speed up computations in the way they have been running for the last decades is by making processors smaller but size reductions necessarily imply a larger number of logic gates per area unit. Making such considerations and if Moore's law is to be followed at some stage the typical circuits dimensions will be in the nanometer scale.

From the theoretical point of view, functioning of processors at this scale is constrained by the physics used to describe the system. At such scale the quantum effects determine their behavior, and these are neglected in current computation. To supply the computational power required also means finding better algorithms to optimize resources in the computing process. Although much research is invested on these issues there seem to be unavoidable limitations and larger operations seem to be doomed to take enormous computing time and resources. Further, also from the technological point of view miniaturization and increasing the computational power offer serious challenges. Miniaturizing the computing components requires, for example, more advanced lithographic techniques, expensive or yet unknown materials, highly controlled fabrication environments, dealing with power dissipation, etc. Assuming that they can be eventually constructed there's still the problem of how to control them once the quantum effects play a significant role since the current scheme is not adapted to deal with a quantum mechanical system.

However, another way to approach the problem is by changing the basic paradigms of the computation scheme. This should not be confused with changing the fundamental basis of computation theory, which has proven to be robust and effective. It seems to be a natural solution to incorporate the quantum effects in the theoretical description of the system and develop a quantum mechanical hardware. This requires to have control over a physical system governed by quantum mechanical rules. During the 1980's the first

theoretical approaches to what is now called *quantum computing* (QC) were outlined and in the last decade an increasing number of research groups have worked out simple models to stress the feasibility of manipulating quantum systems to make computations. They remained as a theoretical curiosity until it was shown that some quantum algorithms could outperform their classical counterparts on problems long studied and that were considered not easily improvable[1]. This was possible because the quantum algorithm used features that are not present in the classical description, namely quantum interference, quantum parallelism and entanglement.

These three concepts are in the core of the quantum computing scheme proposed to solve some of the limitations of classical computing and are the cause for its interesting results. The works by Shor and Grover boosted the research in QC trying to determine to what extent this new approach was useful for solving mathematical problems. Similarly, the quest to find a physical system in which to implement and test such interesting results began. Important results that set the guidelines to define a suitable quantum system to work with as well as the development of basic algorithms framed the basis upon which QC has been grown. Some of these basic elements and tools of the QC approach are discussed next.

1.1 Qubits

The main constituent of QC is the *qubit*, the both physical and abstract entity analogous to the classical bit, where the quantum information is stored. As in the classical counterpart it is described in terms of two fundamental or pure states $|0\rangle$ and $|1\rangle$ analogous to the 0 and 1 classical bits. They represent also the computational basis for the system[2]. The main difference between bits and qubits is that the later can be also in any intermediate state of $|0\rangle$ and $|1\rangle$ described by their linear combination as a result of the superposition principle in quantum mechanics [3]. That is, the wavefunction of the qubit can be expressed in the form

$$|\psi\rangle = \alpha|0\rangle + \beta|1\rangle \tag{1.1}$$

where α and β are complex coefficients satisfying the normalization condition $|\alpha|^2+|\beta|^2 = 1$. These coefficients are the probability amplitudes of the wavefunction and $|\alpha|^2$ and $|\beta|^2$ give the probability for the corresponding state to be found when the qubit is *measured*. It is important to emphasize that even though the qubit can be in a superposition of its basic states, it takes a very well defined value -either $|0\rangle$ or $|1\rangle$- whenever it is measured. This process in which the states goes from a superposition to a pure state is referred to as the collapse of the wavefunction. Yet, the qubit can be manipulated without determining its state and this feature enhances its computational power. It must be kept in mind

[1] In particular Shor's algorithm for factoring an n-digit number and Grover's algorithm for searching through unsorted databases. See references [1] and [2].

[2] The orthonormal basis in the 2D Hilbert space in which the wavefunctions of the system are spanned. This is by no means unique

that qubits are a physical entity which can be fully described mathematically. In principle every quantum system with two well defined states can be used to give the physical description of the qubit and finding the most adequate or promising ones for QC is a major task in fundamental research. Current research focuses on two-level systems defined in trapped ions, cavity QED (quantum electrodynamics), superconducting circuits, semiconductor quantum dots, polarization states of light, the electronic or spin levels of impurities in solids and nuclear spins. Each proposal has features that make it successful and feasible where others fail to some extent but their mathematical description is the same. Additionally, the state of a n-qubit system is described as

$$\begin{aligned} |\psi\rangle &= \sum_{x\epsilon\{0,1\}^n} \alpha_x |x\rangle \\ &= \alpha_{\underbrace{00...0}_{n}} |\overbrace{00...0}^{n}\rangle + \alpha_{00...1}|00...1\rangle + \ldots + \alpha_{11...1}|11...1\rangle \end{aligned} \tag{1.2}$$

where $\{0,1\}^n$ means "the set of strings of length n with each *letter* being either 0 or 1."

1.2 Two-level systems: the Bloch picture

Since there are several candidates for qubits it is desirable to have a general description no matter the system taken and the Bloch picture for two level systems becomes useful and provides also a graphic representation of the qubit. It is taken from the Bloch equations formalism used to describe nuclear spins coupled to static and oscillating magnetic fields. It can be reviewed in [4] but can be understood and used in a quite condensed way by making some modifications to the description of the qubit's wavefunction. Without loss of generality the state of the qubit 1.1 can be written also as

$$|\psi\rangle = \cos(\theta/2)|0\rangle + e^{i\phi}\sin(\theta/2)|0\rangle \tag{1.3}$$

Since $|\cos(\theta/2)|^2 + |e^{i\phi}\sin(\theta/2)|^2 = 1$, in spherical coordinates the angles θ and ϕ represent a point on a sphere of unitary radius. From the previous discussion it is clear that each point on the sphere will represent a different state of the system, which is a superposition of the two basic states except when $\theta = n\pi$ for any $n\epsilon\mathbb{N}$.

So the state of the qubit can be represented by a vector in the unitary Bloch sphere: The north and south poles represent the pure states -the computational basis- $|1\rangle$ and $|0\rangle$. Because of the normalization condition the vector has unitary length. This holds if the state is a *coherent* superposition of the basis states (meaning that the phase relationship between them is well defined) and shrinks for incoherent mixtures. Changes in the length of the vector are caused by uncontrolled interaction of the system with the surroundings inducing decoherence in the description of the system. Finally, the direction of the vector, i.e. the angles θ and ϕ, determine the expectation values of the state as shown in equation (1.3). Using this formalism the manipulations of the qubit can be thought as rotations of the vector in the Bloch sphere.

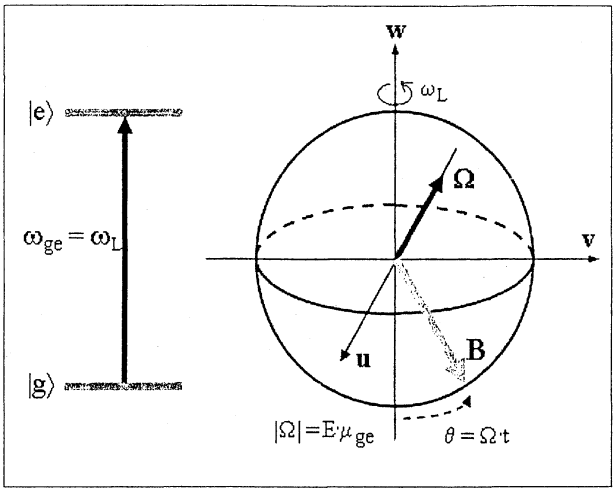

Figure 1.1: A two-level physical system can be pictured as a vector $\mathbf{B}_{ge} = (u, v, w)$ in the Bloch sphere.The vector rotates around a pseudovector Ω pointing in a direction dependant on the detuning of the elecromagnetic field used to drive the transition at a rate proportional to $|\Omega|$. The projection on the w axis gives the population difference of the states. The projections on the u and v axes are related to the phase coherence of the state to the phase of the electromagnetic field.

1.3 Qubit gates

The controlled manipulation of the qubit state by external means define a quantum logic gate. Since in principle there are infinite consistent values for α and β, there can be defined an infinite amount of gates or processes which take $|\psi_{\text{initial}}\rangle$ to $|\psi_{\text{final}}\rangle$. The only requirement for this gates is that they perform a unitary transformation on the state of the qubit in order to preserve the total probability. They are equivalent to carrying out rotations on the state vector defined by the qubit. The Bloch picture exploits this last fact. A particularly interesting transformation is that analogous to the classical "NOT" gate, the one that takes 0 to 1 and 1 to 0. The quantum equivalent referred as *quantum NOT* gate is defined by the transformation $\alpha|0\rangle + \beta|1\rangle \xrightarrow{\text{NOT}} \beta|0\rangle + \alpha|1\rangle$. This gate can be also seen as a 2 by 2 matrix acting on the vertical vector describing the qubit:

$$\begin{bmatrix} 0 & 1 \\ 1 & 0 \end{bmatrix} \begin{bmatrix} \alpha \\ \beta \end{bmatrix} = \begin{bmatrix} \beta \\ \alpha \end{bmatrix} \tag{1.4}$$

This matrix representation can be extended to every other transformation and the only requirement that a valid quantum gate must fulfill is to be described by a unitary matrix.

Although the system described by the qubit can be manipulated to evolve into any given superposition of states not much can be computed with that. In order to make actual computations it is necessary to introduce more qubits to the system and apply multiple qubit gates. The most simple scheme for logic operation can be achieved with a two-qubit description. The general idea behind this is to have at least one of the qubits enabled

to induce changes on the other while being able to control it form the *outside* without inducing decoherence.

One of the simplest interactions between two qubits is that described by a *controlled-NOT* or *CNOT* quantum gate. The CNOT gate requires two inputs, a *control* qubit and *target* qubit. It works by performing a NOT gate on the target constricted by the state of the control qubit. The state of the two-qubit system as given by 1.2 is

$$|\psi\rangle = |\psi_{\text{control}}\rangle|\psi_{\text{target}}\rangle \tag{1.5}$$
$$= \alpha_{00}|00\rangle + \alpha_{01}|01\rangle + \alpha_{10}|10\rangle + \alpha_{11}|11\rangle \tag{1.6}$$

And the CNOT operation is defined by the matrix equation

$$\begin{bmatrix} 1 & 0 & 0 & 0 \\ 0 & 1 & 0 & 0 \\ 0 & 0 & 0 & 1 \\ 0 & 0 & 1 & 0 \end{bmatrix} \begin{bmatrix} \alpha_{00} \\ \alpha_{01} \\ \alpha_{10} \\ \alpha_{11} \end{bmatrix} = \begin{bmatrix} \alpha_{00} \\ \alpha_{01} \\ \alpha_{11} \\ \alpha_{10} \end{bmatrix} \tag{1.7}$$

Interestingly, it has been shown [5] that any multiple qubit gate can be approximated by applying CNOT and single-qubit gates. In the ideal case the system would be isolated and all the process through which the qubit evolves coherently to a different state would be controlled from the outside. Any deviation from this situation introduces errors and information about the state is lost to some extent. If the loss is large then the systems is not usable for computation anymore, although it is also possible to fix the errors if they are traced in parallel. This unavoidable decoherence process sets limitations to the operability of quantum gates. In this context two characteristic times for the system are defined to measure the useful time of the system for quantum computation. The population lifetime, T_1, determines the average duration of the two relevant states of the system. Having long-lived ground states T_1 denotes more specifically the time that can be spent by the system in the excited state before decoherence occurs. On the other hand the phase coherence time, T_2, gives the time for which the phase relation between the qubit states in superposition prevails.

1.4 Generalities

From the fundamental point of view any quantum system with two levels can be used to define a qubit. In order to create a system suitable for quantum computation there are some general directions considered essential to be followed. The so-called *DiVincenzo criteria* aim to summarize all the important aspects that a working quantum computer should integrate. They are discussed in [6] and many works dealing with QC, and a general reminder is presented now.

1. *A scalable physical system with well characterized qubits:* The proposed QC scheme must be based on a physical system that can support qubits with two distinguishable states and be such that several qubits can be put together and used simultaneously.

2. *The ability to initialize the state of the qubits to a simple fiducial state:* In order to proceed with the computation it is first necessary to know the initial state of the system so the appropriate set and order of gates, i.e. the algorithm, can be used.

3. *Long relevant decoherence times, much longer than the gate operation time:* If the phase relations in the superposed state are lost before the algorithm is finished the final measured state cannot be regarded as the outcome of the desired computation. Moreover, if error correction is to be implemented as well, time is needed to trace and correct error sources.

4. *A universal set of quantum gates:* The approach used must define its own way to carry out the transformations on the state of the qubits necessary for computations. As mentioned before, it is sufficient to define the method to implement the single-qubit and CNOT gates.

5. *A qubit-specific measurement capability:* A procedure for reading-out the final state of the relevant qubits must be available after completing the algorithm.

Going from the mathematical description of a qubit and make it follow quantum algorithms to perform computations requires a physical system capable of satisfying the just mentioned guidelines. Finding such a system is perhaps the main task before thinking of all the possibilities and sophisticated features of quantum computing. There exist several interesting proposals of quantum systems that are currently being tested. Most of them have particular features that make them good candidates to satisfy the requirements outlined and although some of them have shown promising results people are still looking for the most adequate one. In particular efforts are being carried out within the approach given by solid state physics in the form of rare-earth ions deposited into inorganic crystals, which is discussed in the next chapter.

Chapter 2

Quantum Computing With Rare-Earth Ions Doped Crystals

The rare-earth ions doped into inorganic crystals are interesting candidates to physically represent a qubit because of several reasons. First, the necessary two levels can be defined in the hyperfine states of the electronic ground state. Also since the ions are fixed inside the crystal no complicated trapping techniques are needed. Another reason is that their ground and excited states show long coherence times when cooled to cryogenic temperatures. This can be useful for quantum computing because then the qubits will have also long lived states, allowing the operation of logic gates. Additionally there is the fact that ions change their energy level structure depending on their position within the crystal lattice. As a consequence there is a way to differentiate each ion (or group of ions) from another according to their resonant frequency spectrum. This enables to selectively address each of them with a particular frequency. How this happens and how it can be exploited is discussed briefly in the next sections and a thorough explanation can be found, for instance, in [7].

2.1 Rare-earth ions

Rare-earth elements or *lanthanides* (RE) are names to describe the group of atoms in the periodic table including those of atomic numbers 57 for lanthanum (La) to 70 for ytterbium (Yb). They share properties that differentiate them from the rest of the elements. They have an electronic configuration of the type $5s^2 5p^6 4f^n 5d^1 6s^2$, where n=0,1,...,13 and corresponds to lanthanum increasing till ytterbium. Their most common oxidation state in solids is the 3+ (customary referred as Re^{3+}), which means that RE ions lose their three outer electrons leading to a configuration ending in a partially filled 4f subshell (except for lanthanum which goes to a closed 5p subshell). Electrons in this shell can be optically excited to higher states, the first of which are $4f^{n-1}5d$, $4f^{n-1}6s$, $4f^{n-1}6p$ and so on. The lower energy 5s and 5p to some extent shield the 4f electrons from the surroundings which has the interesting effect of enhancing the coherence time of the 4f quantum states.

The electronic structure of the free Re^{3+} is a set of manifolds characterized by the quantum

numbers n, l, j, m_j as well as F and m_F to couple the nuclear spin and the total electron angular momentum. Their different allowed values and combinations span a multilevel spectrum consisting of electronic *shells, subshells, terms* as well as *fine* and *hyperfine* structure components[1]. Changes between pairs of such quantum states is regulated by a set of selection rules and thus not all thinkable transitions are permitted. Of particular importance are the electric-dipole (μ) selection rules, in which the coupling between L and S (the resultant quantum numbers of coupling the l and s numbers of all the valence electrons) play a major role in determining which transitions are allowed. For example, dipole transitions in an ion can occur only between energy levels with the $\Delta l = \pm 1$ and the value of L is restricted by this criteria. Therefore dipole transitions between energy levels with same parity are forbidden[2]. The different levels arise from including more perturbing terms into the ion's Hamiltonian. In this way the degeneracy of the general states is removed as more internal interactions of the ion, i.e. more quantum numbers, are considered. It is important to point out that the separation between states might not be readily observable by traditional spectroscopic means since the energy separation between them could be too small.

2.2 Rare-earth-ion doped crystals (REIC)

The just mentioned energy level distribution is consistent with the description of a free ion (or one in an isotropic medium). When this criteria is removed by means of, for example, external electromagnetic fields acting on the ions the rules that determine the structure do not hold but provide a rough approximation. If doped into crystals this effect is specially significant since the ions are in permanent interaction with a crystal field emanating from the surrounding structure. Depending on the intensity of the crystal field on an ion, which is determined by the characteristics of the host as by the particular crystal cell it is embedded in, some symmetries might be broken and the free-ion's states can be split further apart. For example, the *Stark levels* or *Zeeman levels* arise from the interaction of the ions with the electric and magnetic components of the crystal field, respectively. As a result some levels might overlap or become mixed and thus some forbidden transitions become weakly allowed. Furthermore, the effect goes in two directions: just as the crystal field shifts the energy levels of the impurity ions, changes in the electronic state of the ions produce changes in the surrounding field. This effect propagates to the nearby ions coupled to the crystal field and several process in this QC scheme rely on it, as will be explained ahead.

2.3 The REIC quantum computing scheme

As it was said before, when doped into crystals, rare-earth-ions offer a possibility to define a two-level system and hence describe a set of qubits, the building blocks of quantum

[1] A complete discussion on this subject can be found, for example, in [8]

[2] This is not a very strict situation since transitions can become weakly allowed under different circumstances.

computing. It is convenient to start the description of the scheme by looking at the single-ion-doped-in-a-crystal model first and then generalize to the whole crystal with the doping ions randomly distributed in it. The two needed levels can be found, for example, in the hyperfine structure of the ground state of the ions. They show long coherence times (T_2) and correspond to well defined energy eigenstates with well defined excitation frequencies. In general this means that changes in the quantum state -transitions- can be promoted by means of radiation of the adequate frequency, but some considerations should be taken. The qubit states can be conveniently labeled $|0\rangle$ and $|1\rangle$ corresponding to addressable sublevels in the ground state with energies satisfying $E_0 < E_1$. These states also represent one of the possible computational bases.

The particular scheme described uses another state to mediate the transitions between the two basic states already defined. It must be one with a higher energy E_e and optically accessible since it is desired to be efficiently addressed with short-duration light pulses. This additional state can be defined by an excited eigenstate $|e\rangle$ of the ion. Then, the basic model for the system consists of three different levels in the ion where the two levels used for computing, the qubits levels, are connected by a third one only relevant for operational purposes. This means that, for example, in going from $|0\rangle$ to $|1\rangle$ or vice versa in a controlled way the qubit must go trough $|e\rangle$ in a process driven by laser radiation of the frequencies $\omega_0 = (E_e - E_0)/\hbar$ and $\omega_1 = (E_e - E_1)/\hbar$ or equivalently $|0\rangle \xrightarrow{\omega_0} |e\rangle \xrightarrow{\omega_1} |1\rangle$. Although direct transitions between $|0\rangle$ and $|1\rangle$ can be driven using RF pulses, they have the disadvantage of being too slow for the available operation times or being spectrally too broad to address individual qubits independently.

At this point there are two important considerations or reminders for the scheme. One is that the state of the qubit changes in time. Put in another way, it requires some time for the qubits to reach the final state expected according to the followed algorithm. The second is that the qubit can reach a state defined by the superposition of its pure states. Together this means that the quantum mechanical operator acting on the qubits' wavefunction should be time dependant and capable of driving the qubits to any state given by the linear combination of the computational basis. It must also be mathematically expressed as a unitary matrix. It follows that not only the frequency but also the duration of the applied laser beam -the physical operator- shall probabilistically determine the final state of the qubit. That is, the effective time in which the ion interacts with the laser field is such that the final state of the qubit (via the interaction with $|e\rangle$) is $|0\rangle$ or $|1\rangle$ or a linear superposition of both states. Again, this is a major and unique feature of computing with quantum systems. In this way any arbitrary state of the qubit in the given basis can be reached through a series of laser pulses of the right frequency and duration. This process can be regarded as the implementation of a single-qubit operation or quantum gate in the sense of what was explained in 1.3.

The relevance of the pulse duration can be also explained in terms of the Bloch vector picture. For this it is convenient now to remember the concepts introduced in section 1.2 since the three-level system under study can be regarded as two interconnected two-level

systems, for which the Bloch representation is useful. It is clear that taking a Bloch vector from one point to another in the sphere requires an external "force" to be applied over a given interval of time. Using this idea a single-qubit quantum gate can be represented by a series of n laser-driven, non-simultaneous rotations of *two* different Bloch vectors $\mathbf{B}_{0e}$ and $\mathbf{B}_{1e}$ in their own Bloch sphere with poles $\{|0\rangle, |e\rangle\}$ and $\{|1\rangle, |e\rangle\}$ respectively. With each pulse the vector describes an angle θ_n around a direction determined by the phase of the electric field in the light pulse. For example, the steps in which a NOT gate is implemented on the $|0\rangle$ state is equivalent to applying a π-pulse of frequency ω_0 to $\mathbf{B}_{0e}$ which takes the vector to $|e\rangle$. Applying then a π-pulse of ω_1 brings this state down to $|1\rangle$ in the $\mathbf{B}_{1e}$ sphere. The duration of the π-pulse here is quite tautological since it is just as long as needed to take the Bloch vector to the opposite direction. It's also important to remind that $|0\rangle$ and $|1\rangle$ define the qubit, not $|e\rangle$, but a Bloch representation of this qubit in which $|0\rangle$ and $|1\rangle$ are the poles is not easily generalizable because of the intermediate state.

In order to realize logic operations on the system the qubit must remain in a coherent state while it is being used, i.e. it is necessary to keep the quantum state away from uncontrolled disturbances otherwise it is not possible to make accurate predictions on how the state will evolve. Since the pulses require some time to act on the qubit and perform the operation, the time it takes to implement a gate must be shorter than the characteristic useful time T_2 of the system. Pulses or sequences of pulses taking longer than this[3] yield in general no correct results since coherence is lost and the measurable amplitude probabilities of the final state do not provide real information on the process. Thus determining and optimizing this time is of major importance for this approach since it limits the amount of realizable operations.

The next step towards making more detailed manipulations of the qubit and perform some tangible computations is to add another qubit to the system. For the approach under study this means to add another ion. At this stage and for descriptive reasons this extra qubit will be referred as the control qubit of the system. It must be such that it can interact with the primitive qubit in the system (the target qubit), be able to induce changes in it and ready to be externally manipulated. The interaction mechanism is here naturally given by the dipole-dipole interaction of the two ions. The procedure in which the control qubit is manipulated to affect the target qubit goes basically as follows: the crystal field felt by the target qubit includes now the electrostatic field of the nearby control ion. As explained before, the effect of the field is to change the energy separation between the energy levels expected for the free target ion. The control qubit ion experiences now a total field which includes that of the target qubit ion as well. Moreover, since the local environment in the crystal may change slightly from site to site it can be assumed that the transition frequencies are different for each ion. Thus at time $t = 0$ there are 4 optical transition frequencies, namely ω_0^C, ω_1^C, ω_0^T and ω_1^T, where C and T label the control and target qubits. By exciting the control qubit with a laser pulse (ω_0^C or ω_1^C) its permanent dipole moment and electric field change, which changes the overall crystal

[3]Experiments reported in [7] recorded times corresponding to $T_1 \sim 100$ s and $T_2 \sim 500\,\mu$s in Pr:Y_2SiO_5.

field felt by the target qubit inducing a rearrangement of its energy eigenstates. If such a change is large enough then a second light pulse resonant with the original frequencies ω_0^T or ω_1^T can no longer modify the state of the target qubit. Alternatively, if the control qubit is not excited by the first pulse then no shift is induced and the second pulse can still excite the target qubit. See figure 2.1. In this way it can be controlled when a qubit is available for manipulation and when it is not. This mechanism sets the basis in which a CNOT gate is implemented.

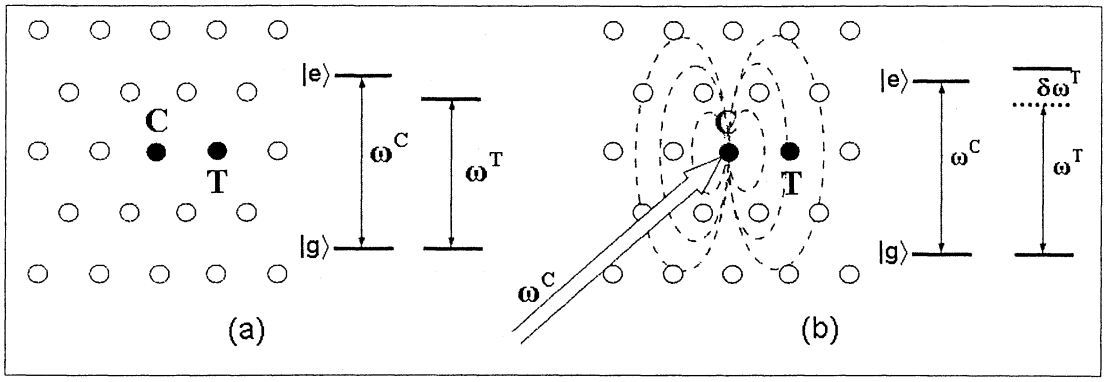

Figure 2.1: (a) In absence of external fields, the ions reach an equilibrium state in the crystal with defined resonant frequencies. (b) When a laser pulse resonant with the excitation frequency of the control qubit the dipole moment of the ion changes inducing a change in the surrounding crystal filed. This propagates to the nearby target qubit ion and ultimately shifts its resonant frequency.

Once an operation has been performed the final state of the two qubits can be readout by different processes, being absorption and fluorescence measurements the most common. For example, to measure the state of the target qubit absorption can be measured by sending light with ω_0^T or ω_1^T and measuring the transmitted intensity of the beam[4]. Work on this has been done previously and is reported, for example, in [7]. On the other hand, fluorescence measurement requires taking the qubit levels $|0\rangle$ or $|1\rangle$ to an excited state and observing the spontaneous emission. To be a measurable effect it is needed that there are many emitted photons.

What has been discussed so far deals with the simple model of two ions with two hyperfine levels in the ground state and a single excited state. Now let's look to a more realistic description of the system. The crystal with the rare-earth-ion impurities has a random distribution of ions in the lattice. The crystal itself also has inhomogeneities in the structure (dislocations, mismatches, additional impurities, etc.) depending on the crystal growth procedure. The direct consequence of such irregularities is a redefinition of the internal states of the Re^{3+} ions due to the effective crystal field (including that of the neighboring ions) in an ample spectrum of energy bands.

[4]However, this requires having much more than two ions in order to have a readable signal. See also the following discussion dealing with the ensemble-of-ions approach.

To use those ions as qubits it is needed that they have known addressable excitation frequencies and that they are close enough as to experience the presence of other qubit ions. It is then necessary to differentiate between the *homogeneous* (Γ_h) and *inhomogeneous* (Γ_{in}) linewidths of ions. The first one refers to the resonance frequency spectrum of a single ion which is slightly wide due to dynamic processes and relaxation; the second deals with that of an ensemble of ions. The inhomogeneous spectrum can be seen also as the sum of the homogeneous ones, as seen in Figure 2.2. In general the amount of nearby ions in the doped crystal is so large that a much broader spectrum of frequencies, i.e. the inhomogeneous linewidth, will induce some measurable excitation.

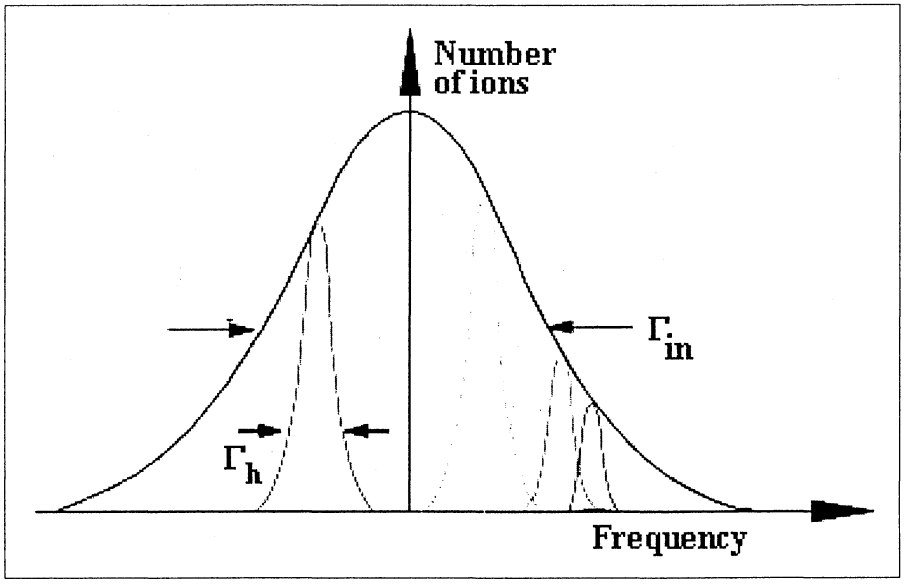

Figure 2.2: According to the position in the lattice and the relative positions of the surrounding doping ions, different groups of qubits have different resonant frequencies. The sum of them, the inhomogeneous linewidth, corresponds to the frequency spectrum of the entire set of ions.

From this excitation spectra broadening follows also that, when implementing actual quantum computing in this scheme, the qubits ions cannot be readily addressed one by one. The system is then described by a set of similar -or equivalent- subsets of nearby ions. These subsets are formed by strongly interacting ions with different transition frequencies (see Figure 2.3) . Each addressable frequency channel is limited by the linewidth of the laser used to drive the transitions. Those qubits absorbing light of the same frequency can be selected from the bulk of ions using *spectral hole-burning* and *optical pumping* techniques as explained in [7]. Also those not suitable for computation can be driven away to auxiliary states by means of a process called *distillation*. The remaining useful subsets work then simultaneously and quite independently just as having many different quantum computers working at the same time following the same algorithm. This is referred as an *ensemble approach* for quantum computing and is not exclusive for the REIC

scheme. During the specific readout of *all* the information-holding qubits the measured signal shall be proportional to the ensemble's average probability of finding ions in the corresponding qubit state. This immediately gives the probability amplitudes of the coherent superposition of states.

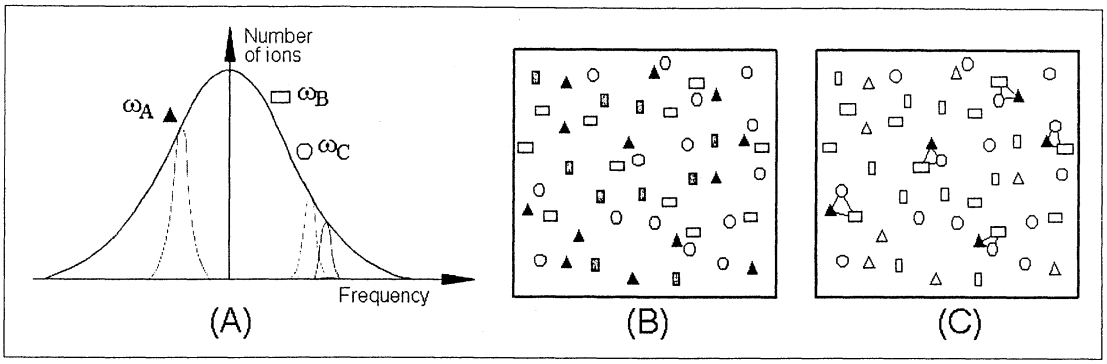

Figure 2.3: (A) Ions resonant with the desired frequencies can be found within the inhomogeneous broadening. (B) Such ions can be addressed in the bulk and (C) those with strong interactions can selected afterwards using spectroscopic techniques.

2.4 Feasibility of the QC-REIC scheme.

To what extent this implementation of a quantum computing scheme is realistic is a matter of current research. However, it has been proven that it can be regarded as a candidate to address certain problems within the general quantum computing field. A way to measure the validity of this approach is consists of applying the DiVincenzo criteria (see section 1.4) to it. Based on the consulted literature the next points summarize the current state of the scheme.

1. Rare-earth ions doped into inorganic crystals have been selected in appropriate groups having two distinguishable and addressable hyperfine states to define a qubit by means of spectral hole-burning and optical pumping. Different groups of similar ions can be selected similarly to increase the amount of available qubits in the system (first criteria). Even so, there is a major constriction for scaling using this procedure: the distribution of ions in the crystal is not completely controlled during doping. In order to create registers with a large amount of qubits it is required that the probability P_i of finding the i-th ion with a different resonant spectrum in the vicinity of the previous $(i-1)$ ions is close to unity so $\prod_i^n P_i \approx P^n$ remains high for large[5] n. Increasing the doping ratio ensures this but it also means that there will be much more than one single ion resonant with each selected frequency in the desired vicinity. This screens the interaction process between ions and blocks the functioning of gates. A possible solution is to go to single ion qubits instead of ensembles, but this is limited by the readout procedure (see fifth point in this list).

[5]The actual size of "high" and "large" is determined by the problem being addressed.

2. Using optical techniques such as optical pumping the ions can be driven to a long-lived, low-energy pure state. By applying this protocol before any other manipulation of the qubit states a well defined initial state is defined. All posterior states achieved through controlled interactions can be measured form this as starting point (second criteria).

3. The qubit states are defined in the hyperfine levels of the electronic structure. Given the structure of the Re^{3+} ions such states are somewhat shielded from uncontrolled interactions with the environment, which means that their relaxation process is slow and he decoherence time is long (third criteria).

4. There are theoretical protocols specifically designed to carry out single-qubit gates on this scheme and whose experimental realization is currently under development. The gates consist of sequences of light pulses of the adequate duration and of the right frequency and the first implementations are expected to be carried out in the near future. Regarding the multiple-qubit gates, the proven selective grouping of ions sets the starting point towards its implementation (fourth criteria).

5. The state of the group of ions defining a qubit system within the crystal can be readout by spectroscopical techniques such as absorption and fluorescence emission (fifth criteria). These techniques are useful in the ensemble since having a large amount of ions in the same final state after the computations ensures a measurable signal approach but this imposes a limitation in scalability.

After this brief analysis it can be pointed out that the scheme has some proven features that make it a suitable candidate for QC implementation. Nevertheless it is also clear that there are still some issues to be explored before final conclusions can be reached. Particularly interesting is the connection between scalability and readout stated in the first and last points. Since without a proper method to extract information all previous computation lacks of meaning. Also, to make interesting or useful computations scalability is a problem that must be solved. One of the purposes of this thesis is to investigate a RE ion with short decay time which is thought to be suitable for enhancing the readout time and capable of storing information about the state of the qubits when co-doped in the crystals. Additionally, this proposal has the advantage of removing some of the problems related to scaling described above. This ideas and some relevant details are discussed in the next chapter.

Chapter 3

Single Ion Readout Scheme

Recent calculations [9] and experiments [7] with Pr:Y_2SiO_5, Eu:Y_2SiO_5 and Eu:$YAlO_3$ have shown that the RE ions can be used to define a qubit system and can be manipulated independently to be taken to a well defined superposition of states as well as being in principle suitable to carry out two-qubit operations. In the ensemble approach described earlier the final state of the qubits can be readout by conventional spectroscopic techniques. However, this approach is inconvenient for scalability (see 2.4) and there is still the problem of ensuring that all the ions in each qubit have the same wavefunction after the computation. These two limitations can be removed using single ions to define qubits instead of ensembles of them. But doing this brings new problems: the long lifetimes of the excited states of the qubit ions are inappropriate for efficient spectroscopic readout. Also the qubits can be trapped in some other hyperfine state and re-excitation can not be grated to increase the luminescent signal. A possibility to overcome such disadvantages of the studied material consists of using an additional RE ion as co-dopant for the crystal to mediate the readout process. This ion, which is not a qubit, should acquire information about the state of the qubit ion and transmit it more efficiently.

3.1 Information transfer and readout protocol

The process used to transfer information from the qubit ions to the readout ions is similar to that used for CNOT gates: once the qubit has been manipulated through logic quantum gates following the desired algorithm a final state is reached. After this a resonant pulse for the qubit ion is sent. Depending on its state, the qubit will or will not be transferred to the excited state. As it was explained before, the transitions in the qubit ion change the local field felt by nearby ions, which includes now the co-doped readout ions. So depending on the resulting state after the pulse the readout ion will or will not have its own resonance frequency shifted as a response to the change in the effective electric field felt (see section 2.2). This change (or the lack of it) can be measured using a second pulse resonant with the transition of the readout ion, thus determining indirectly the state of the qubit before the excitation. Furthermore, this process can be extended to several qubits and current estimations contemplate up to 10-20 qubits. This works by transferring the state of each qubit in the final register sequentially to the qubit ion that controls the

readout-ion, i.e. the one that exerts strong enough changes in its electric configuration, using first CNOT gates and then the previous description. A considerable advantage of this readout process is that it is no longer needed to work with the entire ensemble of ions on the crystal; it is sufficient to find a single group with the desired amount of qubit ions in the vicinity of a single readout ion. This single readout ion can then be excited in cycles in order to produce a strong signal. For this it is necessary that the readout ion relaxes much faster than the qubits.

3.2 Choosing a readout RE-ion

First of all, the readout ion must interact to a measurable degree with a qubit ion within a selected subset of strong interacting qubits. This requirement shall permit to measure differences induced on the readout ion when some information has been passed to it. Second, the readout ion must have two clearly distinguishable (ground and excited) states. With this the information transfer can be traced. Third, the homogeneous linewidth of the readout ion should not be contained in the inhomogeneous linewidth of the subset of qubit ions from which information is to be learned. Otherwise the readout excitation light could also be absorbed by some of the qubits changing the result of the computation. Finally, the excited state of the readout ion must be of considerably shorter duration than the qubit ion. This is perhaps the essential requirement because if it is possible to transfer on them some information about the state of the qubits in the form of measurable changes, such information can then be extracted on the readout ion relaxation time scale instead of the main-dopant relaxation time scale. After research on trivalent RE ions it was found that a suitable one to mediate the readout process was cerium (Ce^{3+}). This ion has a single electron in the 4f shell shielded by the 5s and 5p electrons when in the trivalent state, which means that the ground state has a long coherence time and is not easily disturbed. It also means that the energy spectrum depends only on the values of one electron and can be in principle resolved more easily.

The quantum numbers nlj are used to describe the state of the free Ce^{3+} ($S = 1/2$). Due to the spin-orbit coupling the ground state splits into $^2F_{5/2}$ and $^2F_{7/2}$ levels separated by an energy gap corresponding to $\sim 2000\,\mathrm{cm}^{-1}$ involving no optical transitions between them. Although these states are further split in different *Stark levels* by including the quantum number m_j, the separation of them is small compared to the energy gap. Thus they can be regarded as only two different states with slightly wider homogeneous linewidths (see Figure 3.1). The first excited state for the ion has the valence electron in the 5d subshell and the transitions to this level can be optically driven from the ground state doublet. It is important for the single readout-ion scheme to define the available states within the 5d configuration and how transitions can take place from and to the ground level. Again, for the free ion, the structure in the 5d level is split by the spin-orbit coupling into $^2D_{3/2}$ and $^2D_{5/2}$ fine structure components. Using also m_j in the description these states are split into 4 and 6 different crystal field levels adding up to a total of 10 sublevels in the 5d subshell. Now, in the absence of an external magnetic field the crystal

field states are grouped in doublets, so only 5 sublevels are present. This same effect was neglected in the description of the 4f level.

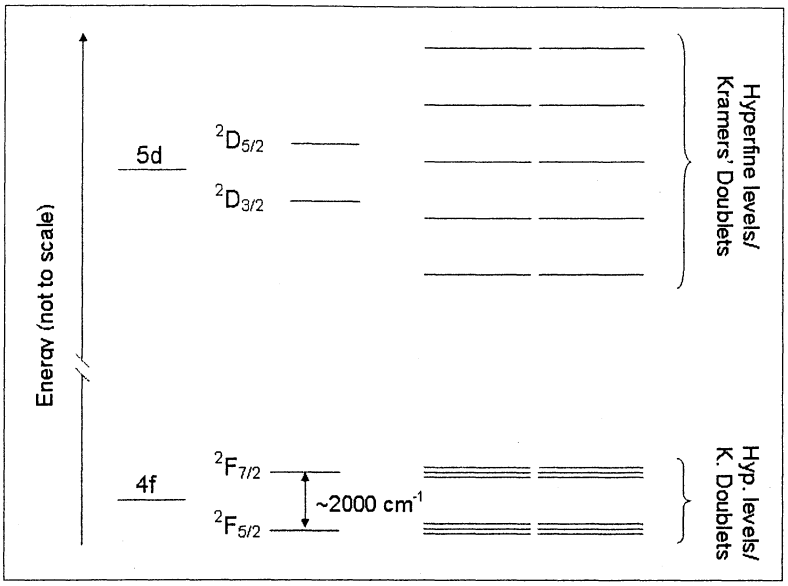

Figure 3.1: The cerium ion energy levels are split apart as symmetries are broken. Transitions in the 4f and 5d subshells are the of major concern for the single ion readout scheme.

The 5d configuration corresponds also to the outermost subshell in the ion. As it was previously discussed, when the ions are embedded in a crystal lattice their electronic structure changes and in this non-shielded state the separations of the sublevels are more vulnerable to changes in the net crystal field. Additionally, the crystal lattice has different phonon modes for the different electronic states of the ions. This means that the lattice vibrates at different frequencies depending on the individual electronic state of all the ions. Equivalently this implies that the electronic level splitting in the ions changes for different vibrational modes. This coupling of the vibrational and electronic levels of the ions in the lattice can be studied using the *Born-Oppenheimer approximation*[1]. With this tool the electronic and nuclear motion are separated and adiabatic changes in the electronic level structure correspond to transitions between the phonon levels. This is valid provided that the difference between the phonon levels (or the difference in displacement around the equilibrium for the initial and final state) is small. Adopting this approximation the free ion model still gives a rough estimation on the electronic configuration of the ions in the crystal. Hence both phonon induced transitions in the excited state sublevels and optical transitions to the ground state sublevels should contribute to the de-excitation of the ion but they can be considered quite independently.

[1]For a thorough explanation see, for example, reference [10]

Chapter 4

Experiments

The main objective of this project is to investigate and provide some information about the trivalent rare-earth ion Ce^{3+} in the context of quantum computing. This is a preliminary and necessary step before using the cerium to co-dope an inorganic crystal to mediate the readout of qubits defined by some other co-dopant RE ion. The cerium was doped into a yttrium oxyorthosilicate (Y_2SiO_5) crystal because some of the results that motivated the exploration of the readout-ion process were obtained from experiments using Pr^{3+} qubits doped in this same host[1]. (See the articles in [7]). The idea behind this is to co-dope a crystal with Pr and Ce once enough information about Ce has been obtained. For doing this it is sufficient to study the behavior of the Ce^{3+} ions as single dopant for the crystal.

At the current stage of the REIC-QC project this thesis is part of, there are some specific tasks to be addressed regarding the single ion readout proposal. For instance it is desirable to check the value of the lifetime of cerium's excited state, which according to literature is around 40 ns [11]. Another important feature to determine is the homogeneous and inhomogeneous linewidths for the ions in the Y_2SiO_5 crystal. It is also necessary to determine the ion-ion interaction to know how close the qubit ions must be located for the readout ion scheme to work. Likewise it is important to find the probability that the Ce ions are captured in a non-fluorescent state, otherwise the final state of the qubits might be biased or remain undefined. This thesis research focuses on the first two of the just mentioned tasks. Originally the outline of the project contemplated addressing more than this. This was not possible to fulfill due to complications with the experimental setup (described below) and the resulting shortage of time. The experiments are thoroughly described in section 4.2 and the results obtained are discussed in chapter 5.

[1] In the crystal growth process used by the manufacturers of the sample the dopant ions substitute a crystallographic site not taken by the Y^{3+}. The notation $(Y_{1.00-x}Ce_x)_2SiO_5$ for the doped crystal makes this clearer.

4.1 Equipment

The equipment used to perform the experiments is listed below. A brief description of the essential components for the setup is provided also. Their functioning is discussed to some extent in the context of the setup but for specific features or instructions the reader is invited to read the cited manuals, data sheets or other references.

1. One $3 \times 3 \times 3$ mm sample of Ce^{3+}:Y_2SiO_5 crystal nominally doped to 0.088%
2. A Coherent CR699-21 continuous-wave single frequency ring dye laser operated with a Coherent 7500 Doubler using a $LiIO_3$ doubling crystal (series 7500-02). The dye laser was pumped with a BeamLok 2060 continuous-wave argon laser and was run using Pyridine 2 dye with a maximum frequency-doubled UV output of 378.85 nm.
3. Wavelength meter (built at LTH).
4. CryoVac helium bath cryostat Type 150.
5. SPEX FluoroLog 1681 spectrofluorometer.
6. Oriel Instruments MS257 spectrograph coupled to an IntraSpec IV CCD camera.
7. A Coherent 7200 Cavity Dumper to control a Spectra Physics 344 acousto-optic modulator (aom), also referred as *Bragg cell.*
8. Miscellaneous: liquid helium and liquid nitrogen, oscilloscopes, photodiodes, photomultipliers, uv lenses and mirrors, etc.

4.2 Description of the experiments

The experiments are presented here in the chronological order they were realized. They were carried out by recording the fluorescence signal from the Ce^{3+} and aiming to provide information on the following issues:

- determining the excitation wavelength and linewidth for fluorescent transitions,
- determining the lifetime of the fluorescent states,
- understand the electronic structure of the excited state and
- finding a zero-phonon line (zpl) for the transition since a narrow line is necessary for the readout.

4.2.1 Emission acquisition

Using the SPEX spectrometer an experiment was carried out to measure the position of the peaks of fluorescence emission. The procedure consisted in exciting the Ce:Y_2SiO_5 sample with a fixed-wavelength light signal selected from an incoherent white light source (xenon arc lamp) using the excitation monochromator. Fluorescence emission was then measured and recorded scanning the wavelength spectrum of radiation coming out of the sample using the emission monochromator in a process known as *emission acquisition* (Figure 4.1. The amount of available excitation and emission light was controlled by two tunable slits after the monochromator pieces. The process was automated by a computer interface where the user sets the desired exciting frequency and the range for fluorescent emission scanning. The different fixed excitation wavelengths used ranged from $\lambda_{ex} = 360\,\text{nm}$ to $\lambda_{ex} = 550\,\text{nm}$ in steps of 10 nm; the fluorescence was scanned from $\lambda_{em} = \lambda_{ex} + 10$, nm to $\lambda_{em} = 650\,\text{nm}$ in steps of 1 nm with a recording time of 0.1 s at each step. The amount of light was regulated using apertures to provide spectral resolutions of 1 nm and 0.5 nm for the excitation and emission slits, respectively. **Note:** the equipment was not calibrated right before the measurements were performed. However, the personnel in charge of its maintenance informed us that it had been recently calibrated and that the measurements should be accurate.

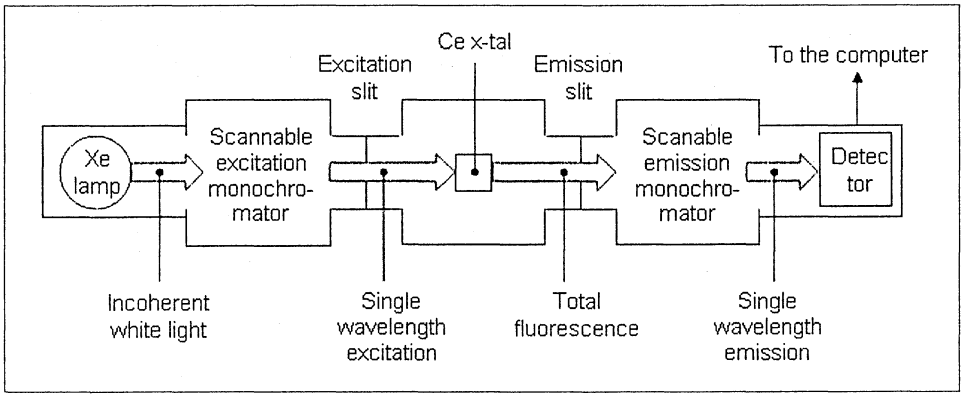

Figure 4.1: Diagram of the SPEX Fluorolog spectrometer. Emission and excitation acquisition experiments were taken to identify emission and excitation peaks in the fluorescence coming from the Ce^{3+} ions in the crystal.

4.2.2 Excitation acquisition

Using again the SPEX Fluorolog spectrometer an *excitation acquisition* measurement was performed during the same session. In this case the emission wavelength was fixed and while the excitation monochromator scanned over a range of excitation wavelengths. The resulting data revealed which wavelengths of excitation are responsible for producing fluorescence of the selected wavelength in the crystal sample. The excitation wavelengths ranged from 350 to 850 nm in steps of 1 nm over a time of 0.1 s each. The fluorescence

wavelengths analyzed were 548, 580, 603, 635, 667, 723 and 869 nm with apertures giving an spectral resolution of 1 nm for both the excitation and emission slits. These wavelength values were not chosen arbitrarily, they corresponded to regions in which some structure seemed to appear during the emission acquisition.

4.2.3 Repetition on emission and excitation acquisition

The fluorescence spectrum from the crystal was broad as expected from the results in literature. Thus it was also necessary to investigate which wavelengths were contributing more to the excitation of the two emission peaks found in the experiment described in 4.2.1. (a) Another excitation acquisition measurement was carried out, now scanning the excitation wavelength from 250 nm (spectrometer lower limit) to 430 nm in steps on 1 nm during 0.1 s and measuring the 396 and 426 nm fluoresced signal. The slits apertures were varied to provide spectral resolutions from 0.2 to 5 nm. (b) A complementary emission acquisition was carried out using excitation wavelength values in the range of 300 nm to 370 nm in steps of 10 nm. The same slit apertures and recording times were used as for the excitation acquisition. These measurements were performed in a second session and after calibrating the equipment and as such the results can be regarded accurate within the device uncertainties.

4.2.4 Excitation acquisition using a laser source

An excitation acquisition experiment was used to test the performance of the dye laser and UV transmittance of the cryostat windows before lowering the temperature of the crystal with liquid He. The laser was operated with a fundamental (locked) wavelength monitored by the wavelength meter while the signal from the frequency doubler output was directed to the crystal mounted inside the cryostat kept at room temperature. A component of the UV beam was measured to monitor the intensity of the signal before impinging the crystal for posterior signal normalization using one of the photodiodes. The resultant fluorescence in the crystal was then filtered with a 400 $\pm$ 10 nm plate such that only wavelengths longer than this value passed. The signal intensity was then measured with the aid of a photomultiplier. The values of the two signals were recorded averaging their intensity on one of the oscilloscopes over 512 cycles to reduce the effect of fluctuations in the background and laser power. The fundamental wavelengths used ranged from 715.5 to 757.0 nm (357.8-378.5 nm in UV output) taking steps of the order of 1 nm. Measurements on the background signals were performed periodically. A diagram of the experimental setup can be seen in Figure 4.2. **Note:** according to the operation manual for the frequency doubler the 7200-03 doubling crystal was needed for the used fundamental frequency. This crystal was not available by the time the measurements were carried out and the 7500-02 crystal was used instead.

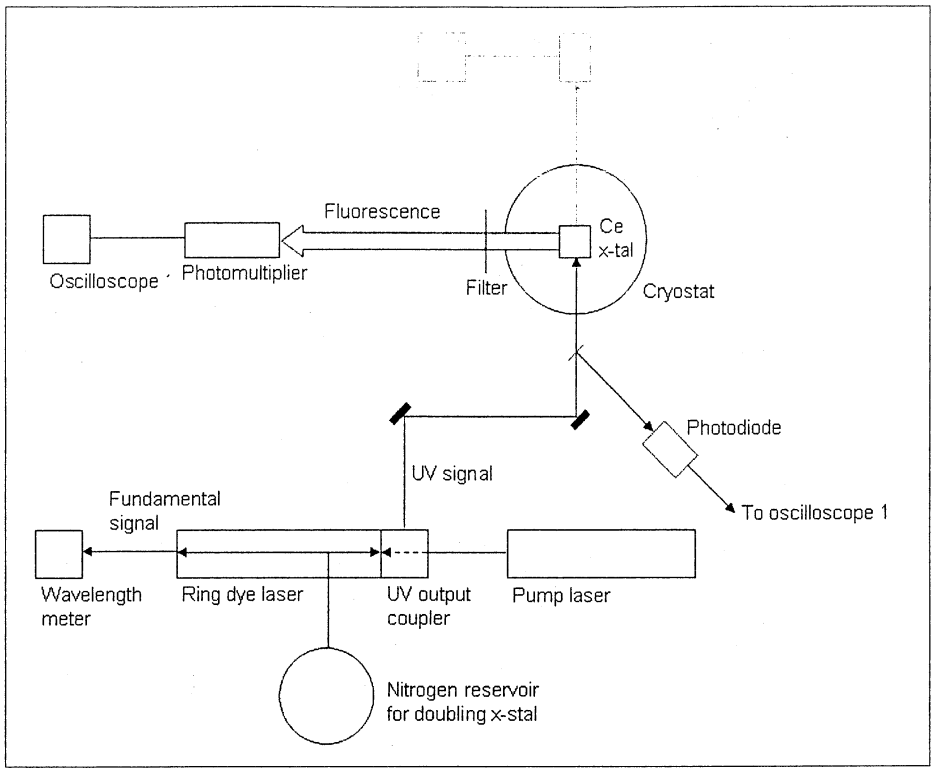

Figure 4.2: Experimental setup used to measure the fluorescence promoted with laser light at room and liquid helium temperatures.

4.2.5 Excitation acquisition using a laser source at cryogenic temperature

Using the same setup as in the previous experiment a new run was implemented to measure changes in the fluorescence spectrum in a temperature of approximately 4 K. The cryostat was cooled down with approximately 12 l of liquid helium and an additional photodiode and oscilloscope were used to measure the transmitted UV signal. The fundamental wavelengths were taken in the 700.7-757.4 nm interval in steps of the order of 1 nm. The values of the three signals were recorded averaging the signal intensity on the two oscilloscopes over 512 and 126 cycles, respectively. As before, measurements on the background signals were performed periodically. This same experiment was repeated with a second helium charge but limiting the fundamental wavelengths interval to 741.2-756.2 nm to determine a possible zpl suggested by the results in the previous experiment. **Note:** the cryostat presented failures probably related to inefficient insulation or helium leakage. These defects were not repaired during the experiments. Consequently the useful time of the helium charge was lowered and a temperature of $\sim$ 4 K could not be maintained or guaranteed during measurement.

4.2.6 Fluorescent states lifetime measurement

To measure the lifetime of the fluorescent states at room/helium temperature an experimental setup as the one schematically shown in Figure 4.3 was used. The acoustooptical Bragg cell together with the cavity dumper driver were used to control the time duration of a diffracted component of the UV beam. This pulsed secondary beam was directed to the crystal just as the single UV beam was directed in the experiments described in 4.2.4. The resultant fluorescence intensity value was averaged over 512 cycles and recorded by a computer linked to the oscilloscope. A single fundamental wavelength of 729.5 nm (364.8 nm UV output) was used and the diffracting action of the aom cell was modulated by an external function generator. Different values for the fluorescence intensity were taken by varying the resistance of the signal at the oscilloscope. The values used were 50, 100 and 500 Ω and 1, 5 and 10 kΩ.

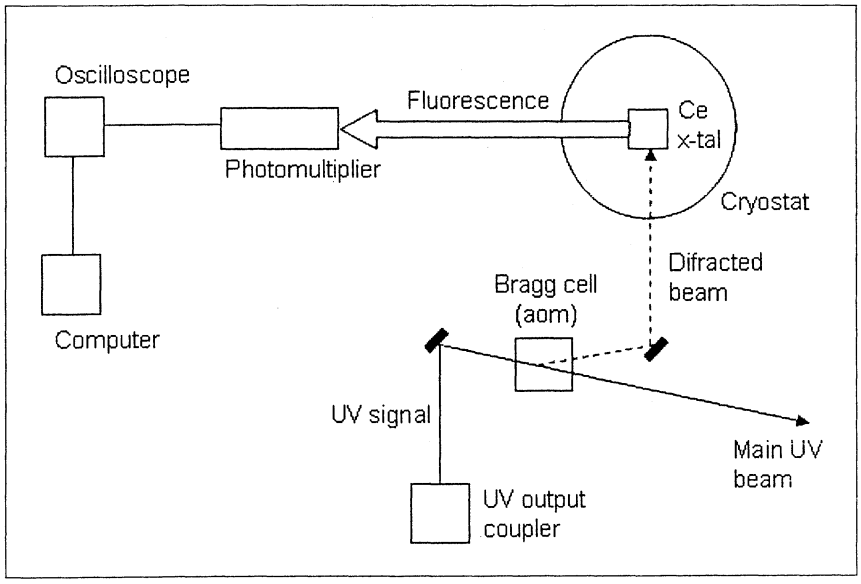

Figure 4.3: Detail of the experimental setup used to measure the fluorescent states lifetime at LHe temperature.

4.2.7 Emission acquisition using a laser source at cryogenic temperature

The last experiment consisted in an emission acquisition measurement on the fluorescence from the crystal at an initial $\sim$ 4 K temperature[2] to search for a zero-phonon line. A 729.5 nm fundamental wavelength was used to produce the UV signal directed on the crystal. The fluorescence was coupled to an optic fiber and directed to the spectrometer.

[2]The temperature at the end of the experiment was not the same because of the problems in the cooling system. See note in 4.2.5

First the background and then the fluorescence were measured and averaged over 3520 cycles at room temperature. Then the cryostat was cooled down with liquid helium and the measurements were repeated. See Figure 4.4.

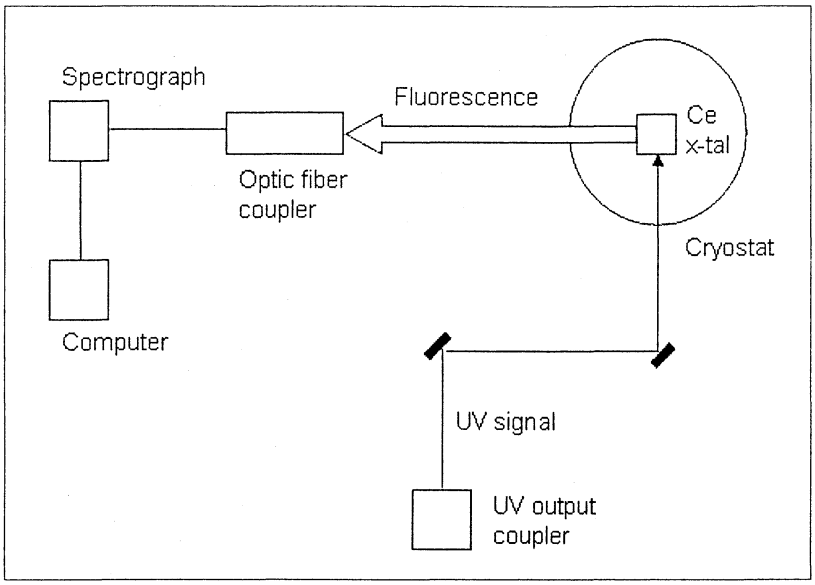

Figure 4.4: Detail of the experimental setup used to search for the zero phonon lines in cooled cerium doped crystal.

Chapter 5

Results and Analysis

The experiments were carried out in the chronological order given in 4.2 with the first immediate objective of with finding the emission peaks of the cerium ions in the YSO crystal. The subsequent experiments followed a practical guideline in which every further step was planned in order to get a more complete understanding of the previous results, to test the hypotheses and to address the project's objectives. However, the analysis of the results can be understood more clearly when all the information is gathered. Some data analysis was done in between the experiments but this was mainly to set the important parameters of the upcoming measurements. Accordingly, the results presented in the next pages do not correspond necessarily to the order in which they were recorded but to the order in which the final analysis was put together.

The first part of the analysis is concerned mainly with the fluorescence emission experiments detailed in 4.2.1, 4.2.3 part b and 4.2.7. Here it is described how the wavelengths of the two main emission peaks for the cerium ions is determined both at room and liquid helium temperature. The presence of these peaks is consistent with transitions to the ground state 4f-doublet for the free ions and reasons for the emission broadening are discussed. Along the way some evidence for a second active luminescent site in the crystal is found while examining the dependance on excitation wavelength for the emission spectra. Finally some measurements are analyzed to determine the presence and wavelength of zero phonon lines for the transitions at cryogenic temperatures.

The second part of the analysis is devoted to the fluorescence excitation experiments, those described in 4.2.2, 4.2.3 part a, 4.2.4 and 4.2.5. With the results obtained it is possible to determine the Stokes shift of the cerium ions, i.e. the difference between their emission and excitation (absorption) band peaks. Some information about the structure of the 5d subshell is revealed using short excitation wavelengths, whereas confirming evidence for the second luminescent site is obtained from high excitation wavelength measurements. The search for zpl is addressed once more in the spectra recorded at liquid helium temperature using the UV laser source with similar results as before and some final comments on the broad excitation profiles close the section.

Finally, in the last part of this chapter the mean lifetime of the excited 5d sublevel is determined from the data taken at liquid helium temperature. The experiment analyzed this time is the one in 4.2.6.

5.1 Fluorescence emission.

The data taken in the fluorescence emission measurements provided some interesting information on the de-excitation process of the cerium ions in the crystal. The results are partially presented in Figure 5.1. The first thing to notice is that the amount of fluorescence light is higher for shorter excitation wavelengths in the 360-550 nm interval. It is also observable that the intensity changes considerably from $\lambda_{ex} = 370\,\text{nm}$ to $\lambda_{ex} = 380\,\text{nm}$ and thus is clear that the main excitation bands for both emission peaks lies at shorter wavelengths than 380 nm. Second, it was shown from the data plots in that the spectral width is close to 70 nm, ranging from approximately 390 to 460 nm for the average full width at half maximum (FWHM) values. This means that there is a broad band of fluorescent transitions taking place in the crystal. There are several ways to explain this is and they will be addressed next. First it is necessary to point out that the exciting frequency spectrum is broadened by the aperture in the slits. Narrowing the slit produced indeed a finer excitation spectrum but the ratio of background noise and fluorescence detected was not good enough as to get a clear emission profile. Nevertheless, this technical limitation is of minor importance and sets only the limit of how narrow can structures be resolved in the spectra, which was found to be of 1 nm. A more important factor is the density of phonons per vibrational state in the crystal. Its abundance is determined by the temperature of the crystal and for room temperature the levels are highly populated. This means that the ions emit and absorb phonons in the ground and excited electronic states when the 4f-5d transitions take place. This broadens both the emission and excitation spectra. To understand better the data obtained it is instructive to analyze the spectra in sets of similar profiles.

The highest intensities recorded for emission were achieved with the wavelengths $\lambda_{ex} = 360\,\text{nm}$ and $\lambda_{ex} = 370\,\text{nm}$. Curves in Figure 5.2 show a broad emission spectrum for both exciting wavelengths although a maximum could be seen for $\lambda_{em} = 397\,\text{nm}$ and some not so sharp structure also around $\lambda_{em} \approx 422\,\text{nm}$ in the FFT-smoothed profiles. According to literature the last one should be a peak too. The mean separation of these peaks has been reported to be in the 2000 cm^{-1} regime. Although the measured separation between the peaks in figure 5.2 it is not clearly defined the rough estimation of $\simeq 1500\,\text{cm}^{-1}$ in general agreement with the values reported previously.

The broadness of the spectrum indicates that there are different optical transitions taking place in the cerium ions. This is either due to the inhomogeneous linewidth broadening, the different phonon levels in the crystal or a combination of both. However, the two peaks suggest that there are two preferred transitions and they correspond to those going from some mean phonon level in the lowest electronic sublevel of the 5d subshell to some

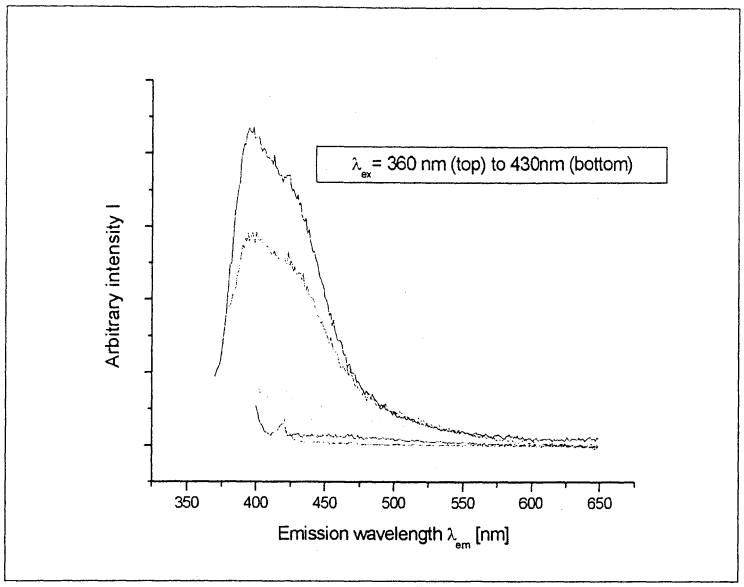

Figure 5.1: Emission spectra for different excitation wavelengths. The highest intensity corresponds to $\lambda_{ex} = 360$nm and decreases monotonically thereafter. In the plot excitations down to 430 nm are shown. Measurements down to 550 nm were performed with no further gain in information.

other mean vibrational level[1] in the fine structure levels of the 4f subshell, $^2F_{7/2}$ and $^2F_{5/2}$, as schematized in the configuration coordinate diagram shown in Figure 5.3. Here it can be seen how the 4f-5d transitions in the cerium ions go from the ground state to some phonon level in the excited electronic state. The lattice then rearranges through a phonon induced process (as described by the Born-Oppenheimer approximation) to reach a mean vibrational state. The ion then relaxes to some vibrational state in the electronic ground state emitting a photon. Transition to different phonon levels is one of the reasons for broadening in the emission spectra. As a reminder to the reader, the energy difference between the mean excited sublevel in 5d and the $^2F_{5/2}$ state is larger than that to $^2F_{7/2}$ so the transitions ending in the former state are those emitting light of $\lambda_{em} \approx 397$nm and consequently those ending in $^2F_{7/2}$ emit light of $\lambda_{em} \approx 422$nm.

The next measurements using $\lambda_{ex} = 380$, 390 and 400 nanometers produced a spectrum of different shape with interesting features as is shown in Figure 5.4. Although their intensity is much lower and the details at shorter wavelengths than 400 nm cannot be measured because they are screened by the transmitted light, they showed an unexpected peak of fluorescence at $\lambda_{em} = 419$ nm that could not be resolved previously. A first suggestion to explain this peak was to label it as the transition from the excited state to the $^2F_{7/2}$ level that could not be clearly determined earlier. If so there is a separation between peaks, i.e. between the ground state sublevels of 1300 cm^{-1} which might still be within the range

[1] It is expected that those mean values get closer to the lowest vibrational levels as the phonon density is decreased.

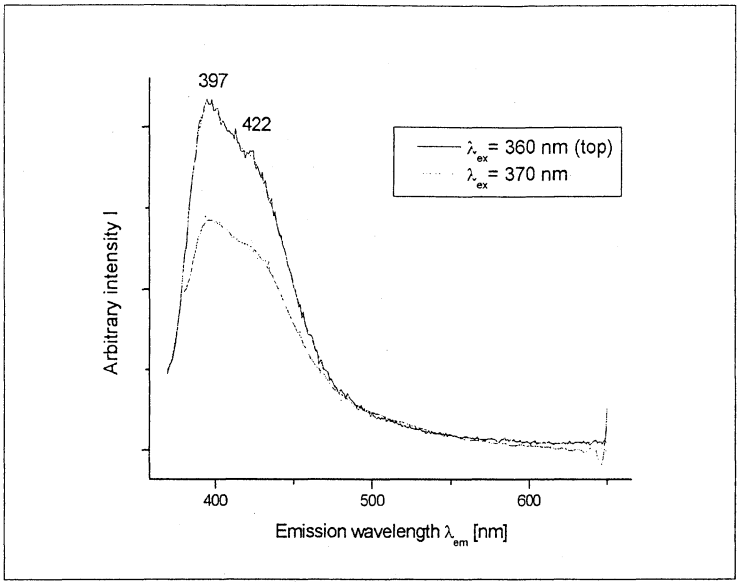

Figure 5.2: Emission spectra for $\lambda_{ex} = 360$nm (highest intensity) and $\lambda_{ex} = 370$nm together with their FFT-smoothed profiles. The emission peaks at 399 nm and ~ 422 nm.

of the reported values. However, it is strange that there is no contribution at all coming from the relaxation to the $^2F_{7/2}$ which rise suspicion on the previous statement. Other explanations such as a different optical process, contribution from accidental dopants or a zpl for the second peak were suggested as well but no clear conclusions could be derived.

The less intense spectra recorded used exciting wavelengths in the 410-550 nm interval. Although the experiments were more concerned on the process generating the two emission peaks at $\lambda_{em} = 397$ nm and $\lambda_{em} = 419$ nm it was also interesting and important to look for some other, though less intense, peaks in the fluorescence. During these last measurements several particular points that seemed to have some structure were roughly determined. The main criteria followed was the relative intensity of the "peaks" as well as the persistence as the excitation was changed. The most significant were located around 548, 580, 603, 635 and 667 nanometers. According to the consulted references there are no transitions in this range except, maybe, for the case of $\lambda_{em} = 580$. Later on these wavelengths were also checked against the UV xenon arc lamp spectrum to discard transmission on the crystal as a source of the structure but no matches were found. Finally some check against the fluorescence spectrum of Eu^{3+} and Pr^{3+} which suggested that there might be some accidental doping of these ions. These emission wavelengths were later also used in one of the excitation experiments and the details of the analysis are presented in the next section.

In the plots shown in 5.5 the intensity of the fluorescence emitted while exciting with

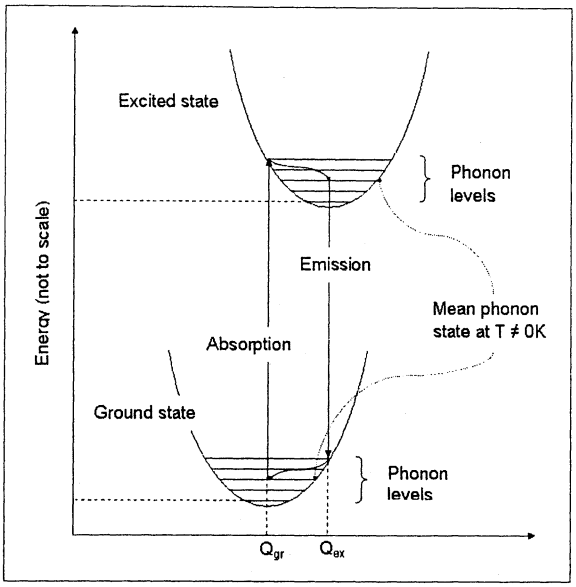

Figure 5.3: Transition to different phonon levels is one of the reasons for broadening in the emission spectra. The configuration coordinate Q gives the mean separation between the optically active ion (Ce^{3+}) and the neighboring crystal ions. The difference between Q_{gr} and Q_{ex} is due to the difference in coupling of the cerium ions and the lattice for the ground and excited states.

short wavelengths[2] is presented and they complement the information enclosed in Figure 5.1. At first sight the overall behavior of the emission resembles the one seen for longer excitation wavelengths: the profile remains broad, the peaks are in the same region, and the intensity is maximum for excitation wavelengths around the 360 nm. Nonetheless it is important to notice that the main peak appears at a different position than in the previous plots. Two factors that might have contributed to such result are having re-calibrated the spectrograph between the series of measurements as well as changing the aperture of the slits (mainly for the excitation light inlet).

In spite of the similarities, there are more things to be learned from these series of data. For example, from the plots corresponding to $\lambda_{ex} = 350$, 360 and 370 nm it can be concluded that the intensity changes more rapidly for higher than for lower excitation wavelengths. It can also be noticed that the plots for $\lambda_{ex} = 320$ and 330 nm are quite odd in comparison to the shape of the rest. This dissimilarities can be appreciated more clearly in figures 5.6 and 5.7. A possible explanation for the differences in these spectra is suspected to be related to having different fluorescent *sources* in the crystal: searching in literature it was found that the material used as well as the crystal-growth technique employed (as given by the crystal data sheet) allow two different crystallographic configurations for the Ce^{3+} ions [12]. According to their discussion these two sites have a different luminescent behavior and in particular they emit strongly at different wavelengths but with unmatched relative

[2]By *short* it is meant shorter than the wavelength of the emission peaks.

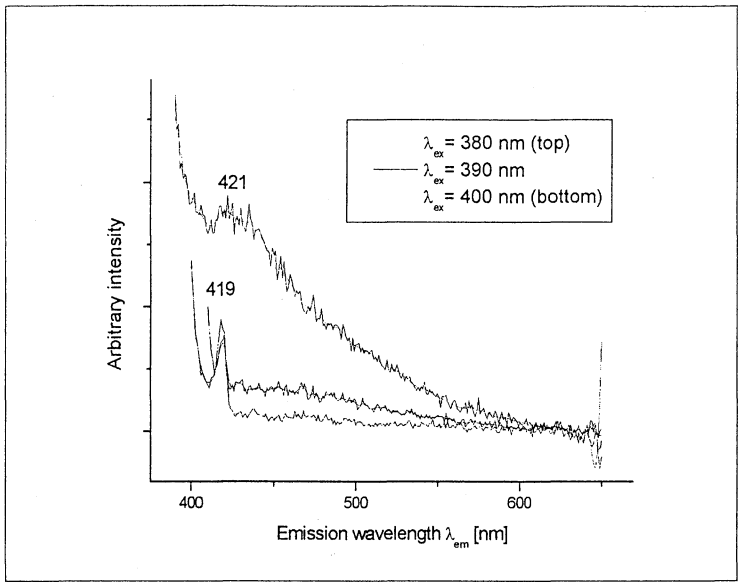

Figure 5.4: The measured and smoothed emission spectra for excitation around $\lambda_{ex} = 390$nm clearly identifies the peak going to the $^2F_{7/2}$ state at $\lambda_{em} = 419$nm.

intensities. Furthermore the main luminescent site is said to emit strongly in the 400 nm region while the second and less intense site is peaked in longer wavelengths somewhere in the 500 nm region.

If this is the case given the crystal sample used, it might be possible to observe a signal from the second site at excitation wavelengths lower than 500 nm just as it is possible to see a signal for lower than 400 nm from the main site. This might be particularly true when λ_{ex} is taken around the 320-330 nm interval, where the intensity of the emission from the main site seems to be low. With the available information so far is not possible to draw conclusions about this unexpected behavior but the results from the excitation experiments presented in section 5.2 shall provide some additional information on this and other matters.

Once the emission peaks were determined the experiments took a different direction. Another objective of the project is to determine the zero phonon lines of the ions in the crystal. One of the attempts to address this task consisted in repeating the fluorescence emission measurement having the crystal in a liquid helium bath in order to minimize the thermally created phonons in the electronic sublevels of the ions. This time the ions were excited with $\lambda_{ex} = 364.78\,\text{nm}$ laser ligth[3] and the profile obtained as well as one taken at room temperature for comparison is shown in Figure 5.8. Although the signal for the fluorescence and the background were integrated over long periods of time (corresponding to over 3500 measurement cycles) to minimize fluctuations, the signal presents a noisy

[3]This value corresponded to the highest UV output power from the dye laser.

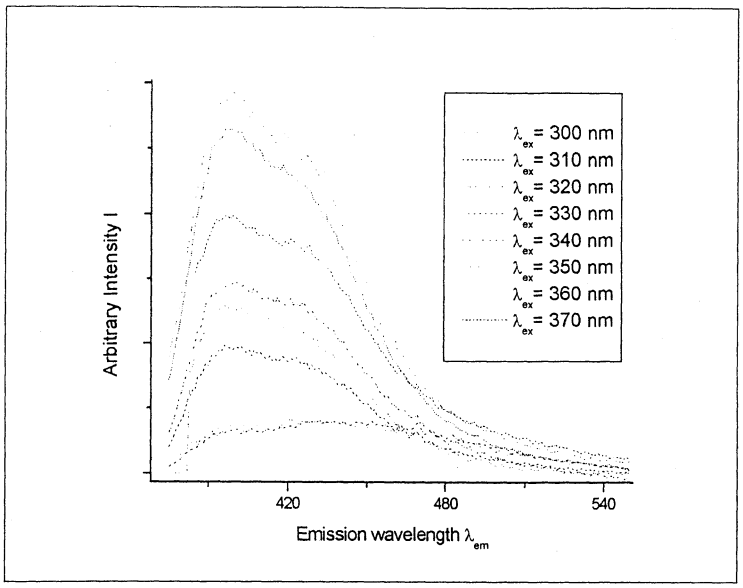

Figure 5.5: Emission spectra for low excitation wavelengths. Once again the highest intensity corresponds to $\lambda_{ex} = 360$nm and decreases to both sides. The peaks appear shifted from the previous values found as a consequence of setting different values in the parameters of the spectrometer. See also Figure 5.6.

profile. It is suspected that a malfunctioning of the equipment is the main cause for the low accuracy of the measurement. The peak corresponding to the scattered laser light at $\lambda_{em} \simeq 365\,\text{nm}$ gives the resolution of the device used to record the spectra. The FWHM value of this peak is 0.76 nm and assuming a narrow laser signal (the laser frequency drift is approximately 20 MHz in 20 minutes) the broadening of the peak is then caused by the spectrograph grating. This sets a lower limit for readable fluorescence signals which. Narrower structures than this value cannot be resolved and they will appear as structures with the same FWHM provided the signal intensity is strong.

The zero phonon line transition probability is low for high temperatures because the phonon emission-absorption process within the electronic subshell levels leave the ions around an undetermined average phonon state. However, the phonon density per state in the 4f and 5d electronic subshells is expected to approach zero as the temperature is decreased to 4 K and the ions will be in the lowest vibrational state before the optical transition. Further, having less phonon levels available might increase the chances to reach a zero phonon level as well if there is some overlap of the wavefunctions in the vibrational ground level in both electronic states.

If the inhomogeneous excitation linewidth broadening is also decreased with temperature[4], a peak in emission corresponding to zpl occurs because of the de-excitation of a large amount of ions emitting on the same wavelength. On the other hand, if the inho-

[4]This is discussed for the excitation experiments in 4.2.5.

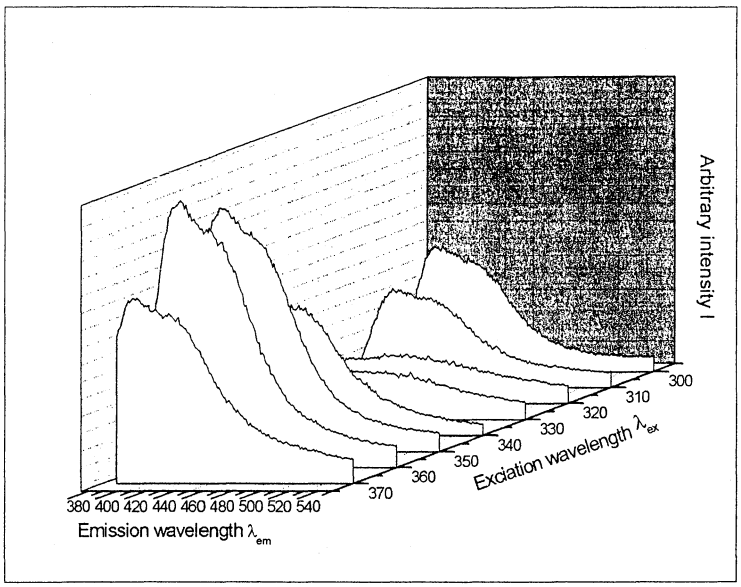

Figure 5.6: Perspective view of the emission spectra for low excitation wavelengths. The shape of the plots for $\lambda_{ex} = 320$ and 330 nm shows different features than the rest suggesting a different emission process taking place.

mogeneous linewidth remains broad the individual zpl of different groups of ions in the crystal ensemble might not be intense enough as to stand in front of the fluorescence signal from the rest of the ions undergoing phonon and optical transitions together. Figure 5.8 shows no discernable peaks between the excitation and major peak wavelengths, where the zpl lines should appear. One possible cause for this is that the inhomogeneous linewidth does not get thinner as it was explained before. An additional cause might be an experimental failure. As it was mentioned in 4.2.5, there were cooling deficiencies suspected to have occurred while the measurements were taken. This might decrease the chances of having a strong emission signal for the zero phonon transitions. There is also the possible malfunctioning of the spectrograph pointed out earlier.

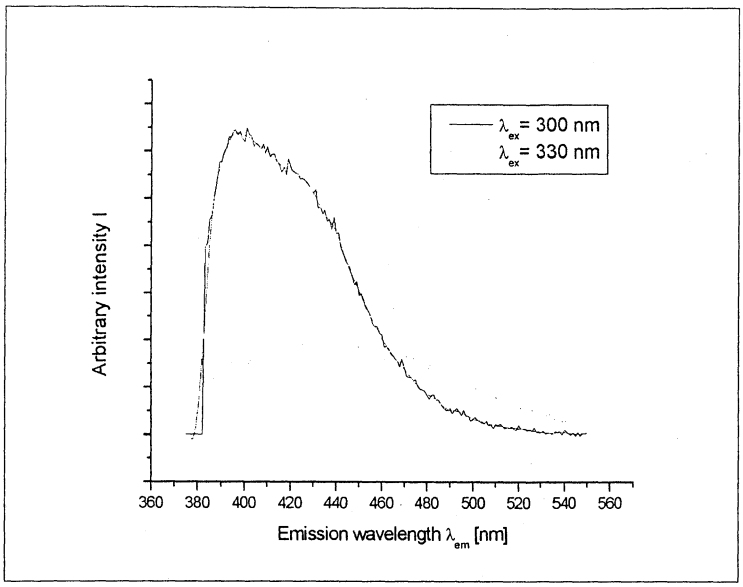

Figure 5.7: Two plots of comparable intensity feature marked differences in shape. While the one with $\lambda_{ex} = 300\,nm$ repeats the pattern observed in most of the plots analyzed, the one with $\lambda_{ex} = 320\,nm$ seems to be shifted to higher emission wavelengths and with a more uniform distribution of intensities.

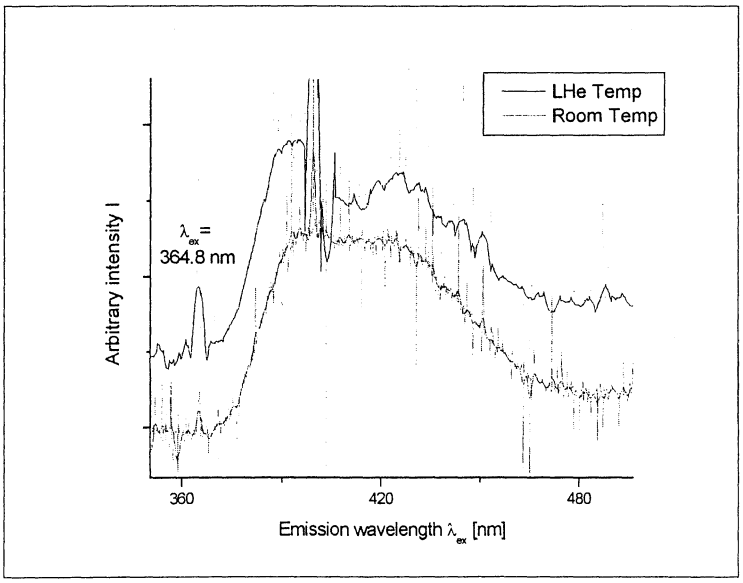

Figure 5.8: The spectrum taken at liquid helium temperature (top) presents a noisy profile and no well defined zpl can be observed. A malfunctioning spectrograph might be one of the causes.

5.2 Fluorescence excitation.

The information obtained from the excitation experiments complement the one gained in the emission measurements and provides a better understanding on the fluorescence and vibrational processes of the cerium ions in the crystal. By examining the position of the fluorescence peaks as a function of the exciting wavelengths it was pointed out that the ions in the crystal were absorbing and emitting in quite different wavelength bands. The excitation was scanned to determine the location and broadness of such bands by looking on the emission[5] in $\lambda_{em} = 396\,nm$ and $\lambda_{em} = 426\,nm$. The recorded spectra for the 396nm output consisted of the three broad peaks centered at 267.5, 300 and 359 nanometers plotted in Figure 5.9. From this structure and the previous results several things can be learned. Perhaps the most obvious is that the inhomogeneous linewidth that creates transitions in the ions that decay emitting light of 396 nm is broad at room temperature and has several local maximum values. This means that there are many different excitation channels to promote 4f $\rightarrow$ 5d excitations in the crystal. The portion of the profile going from $\lambda_{ex} = 300\,nm$ to 370 nm is in agreement with the spectra coming from the emission experiment (see Figure 5.5) in which the highest intensities were obtained form excitations in the 350-370 nm band and quickly lowering on both sides and rising again at 300-310 nm. These multiple peaks also reveal information about the structure of the 5d subshell. The three bumps indicate that there are three observable sublevels in the excited 5d state from which the ions decay again to the ground level.

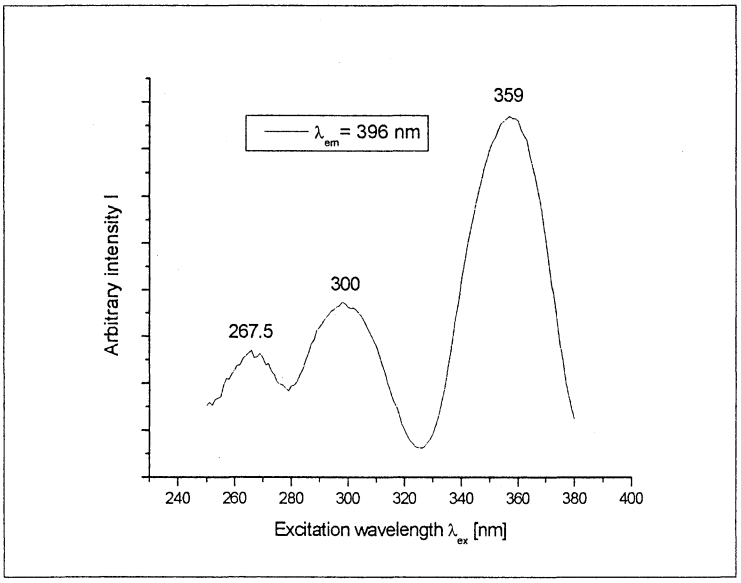

Figure 5.9: Excitation spectrum for $\lambda_{em} = 396\,nm$ fluorescence. The multiple peaks help determining the electronic structure of the 5d subshell.

[5]The emission wavelengths were intended to coincide with the values previously found for 397 nm and 422 nm, but by the time the experiments were run those values had not been precisely determined.

Comparing this data with the previous results as in figure 5.10 it is clear that the emitted light is less energetic than the absorbed one. This clearly demonstrates that non-optical processes are occurring. They must take place within the electronic sublevels where the internal vibrational structure allows phonon emission and absorption. Since most of the 5d $\rightarrow$ 4f transitions go from the lowest sublevel of the 5d electronic manifold, the excitation band centered at 359 nm should be regarded as the excitation band that generates transitions from the ground state to the lowest level in 5d; the other bands do the same for the higher levels. The peak-to-peak difference between the 359 nm excitation band and the emission spectrum provides a good estimation on the *Stokes shift* for the ions, i.e. the difference between the absorption and emission energy band peaks linked to the displacement of the ions in the lattice for different electronic configurations. The value found for the Stokes shift was 2600 cm^{-1}. Furthermore, the peak values set the energy difference between this ground level component and the three lowest levels in the 5d electronic manifold. (See also Figure 5.13.)

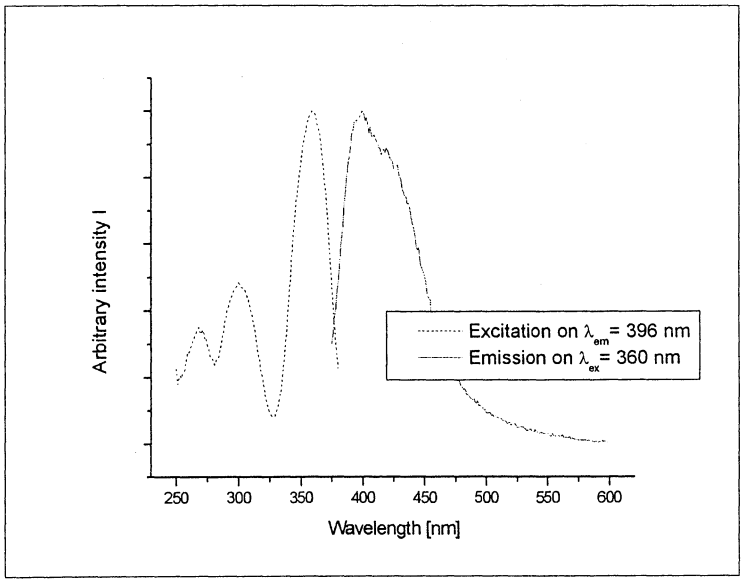

Figure 5.10: A comparison between emission and excitation spectra shows that the ions absorb and emit photons of different wavelength. Vibrational processes in the electronic sublevels are held responsible for the energy dissipation.

The broadening in the 359 nm excitation band may be caused by the inhomogeneous linewidth as well as from transitions taking place from different vibrational states around the mean values present at room temperature in the electronic ground level. This same reasoning applies to the broadening around 298 nm and 267.5 nm but there might be some other causes as well, particularly the overlap of phonon levels from different electronic sublevels in 5d. In this sense the peak values give the separation between the equilibrium phonon states in 5d and $^2F_{5/2}$.

It is useful to look again on 5.10 and compare the broadening of both profiles. For the emission spectra, the FWHM was found to be around 68.6 nm while the one for the 359 nm excitation band is 32.1 nm. However, one should keep in mind that the emission spectrum corresponds to the overlap of two broadened transitions to the ground state doublet of at least one luminescent site. The total spectra is quite symmetric and it is reasonable to propose a decomposition on two gaussian profiles (figure 5.11). Assuming similar FWHM values for them, it is clear that each signal would have then a broadening of $\sim$ 34 nm, just like the excitation profile. This can be interpreted by saying that the distribution of phonon states is similar in both the excited and ground electronic states (equally separated vibrational levels).

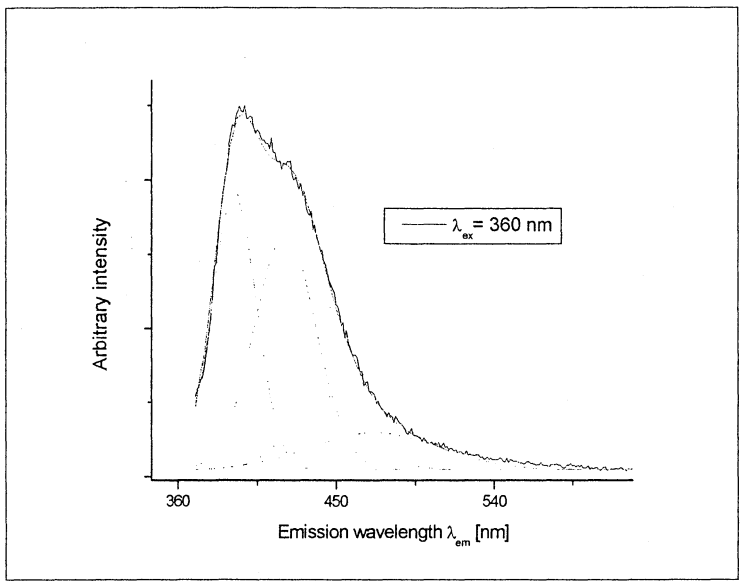

Figure 5.11: The emission profile can be approximated by the overlap of gaussian curves with similar FWHM values. Two additional curves were needed for the approximation. Their contribution is more evident for longer wavelengths beyond the two peaks region and its implications are discussed ahead.

On the other hand, the excitation spectrum obtained for $\lambda_{em} = 426$ nm (Figure 5.12) was expected to have the same shape as the one taken for 396 nm since it is assumed that most of the 4f $\rightarrow$ 5d transitions start in the $^2F_{5/2}$ level because the $^2F_{7/2}$ is expected to be almost empty at room temperature [13]. The data showed essentially the same features as the previous but with slightly shifted peaks centered around 302 nm and 359.5 nm (the third peak was not scanned). The last one gives an estimated average separation of the lowest sublevel of the 5d manifold to the $^2F_{7/2}$ level in the same fashion as before. This spectrum was recorded scanning the excitation wavelength up to 410 nm and showed an extra peak-like structure at 399 nm. Interestingly this peak is located in the vicinity of the major emission peak but cannot be immediately regarded as fluorescence of the decay to the $^2F_{5/2}$ state. It cannot be said either that this is a process originated by a zero

phonon transition since at room temperature the phonon density of the crystal is large. With all these considerations together with the 1500 cm-1 separation between the 4f

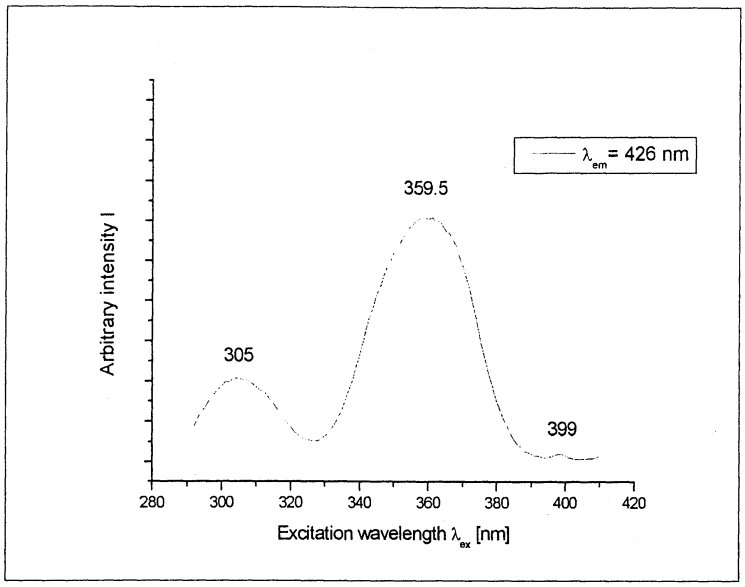

Figure 5.12: The excitation profile for $\lambda_{em} = 426\,nm$ collects the excitation from the 5d $\rightarrow^2 F_{7/2}$ transition. The pattern in Figure 5.9 is repeated with a slight decrease in the intensity as expected from the different intensity of the peaks.

sublevels given in section 5.1, a general description of an atomic model for the ensemble of ions in the crystal can be constructed. The results are shown in Figure 5.13.

It was also interesting to explore the excitation behavior for wavelengths beyond the emission peaks once their origin was understood. Consequently, excitation spectra for long emission wavelengths ($\lambda_{em} > 500\,nm$) were taken trying first to determine if the low intensity peak-like structures observed for the emission gathering corresponded to some unexpected transitions in the crystal. The emission values used were the wavelengths given in 4.2.2 because some sort of pattern was thought to had been found there. It was immediately determined from the data in Figure 5.14 that such bumps are not produced by long wavelength transitions because the most intense peak in their excitation profile is centered around $\lambda_{ex} = 370$. Looking back on the emission results using this same wavelength (see Figure 5.2) there are no identifiable peaks at the analyzed emission wavelengths. Most likely the "peaks" correspond to fluctuations in the light source intensity or in the background signal or accidental additional dopants. However, the following interesting result was observed from these plots.

The first thing to be noticed from the spectra shown in figure 5.14 is that the four of them show a peaked structure for excitations around 370 nm. The highest of these peaks corresponds to the shortest emission wavelength examined of 548 nm. For the rest the intensity of the peak decreases by increasing λ_{em}. The position of the peak indicates

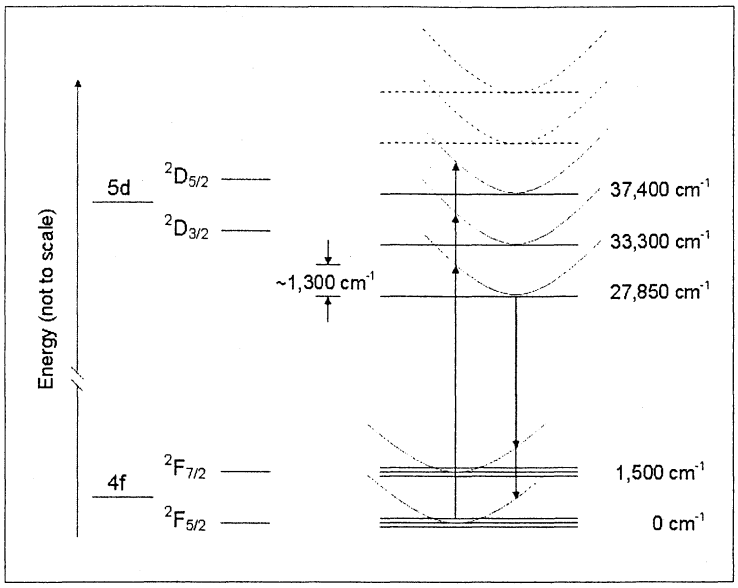

Figure 5.13: The transitions occurring in the ensemble can be pictured using the information from the emission and excitation spectra. The three levels in 5d are defined by the three peaks in Figure 5.9 while the two levels in 4f are given by the two emission peaks. The phonon levels spreading corresponds to the broadening of both types of spectra.

again that there are non optical relaxation processes taking place in the cerium ions: because most of the observed fluorescence is peaked around the 397-422 nm interval and the excitations that promote more fluorescence are peaked around 370 nm, there must be some dissipation of energy $\sim \hbar c/\lambda_a$ and $\sim \hbar c/\lambda_b$ between the excitation and emission processes, with $\frac{1}{\lambda_a} \approx \frac{1}{397} - \frac{1}{370}$ and $\frac{1}{\lambda_b} \approx \frac{1}{422} - \frac{1}{370}$. This is in direct connection to the phonon assisted processes occurring while the ions get to the equilibrium vibrational states mentioned earlier. After comparing the spectrum with those in figure 5.9 it is also noticeable that the highest excitation peak (359 nm) is now located around 370 nm.

It is possible also that the 359 nm peak and these ~370 nm peaks are not the same though. It could be a different excitation spectrum peaked around 370 nm and caused by a second luminescent site of the Ce^{3+} ions in the crystal. If this is true then the spectra in Figure 5.14 corresponds to the excitation profile of a second site while the one obtained for $\lambda_{em} = 396$ nm and 426 nm (Figures 5.9 and 5.12) corresponds to the main site being excited. In [14] it was found that excitation peaks should appear around $\lambda_{ex} = 320\,\text{nm}$ and $\lambda_{ex} = 370\,\text{nm}$ observable at 11 K for $\lambda_{em} = 500\,\text{nm}$. The last peak can be linked to the data in Figure 5.14. The peak in 320 nm cannot be seen directly form the other excitation measurements. Also in the previous section it was said that there were some oddities in the emission spectra when the material was exited with 320-330 nm light and those differences were stressed in Figure 5.7. In order to find out more about the differences in the emission structure it is convenient to integrate the total intensity of

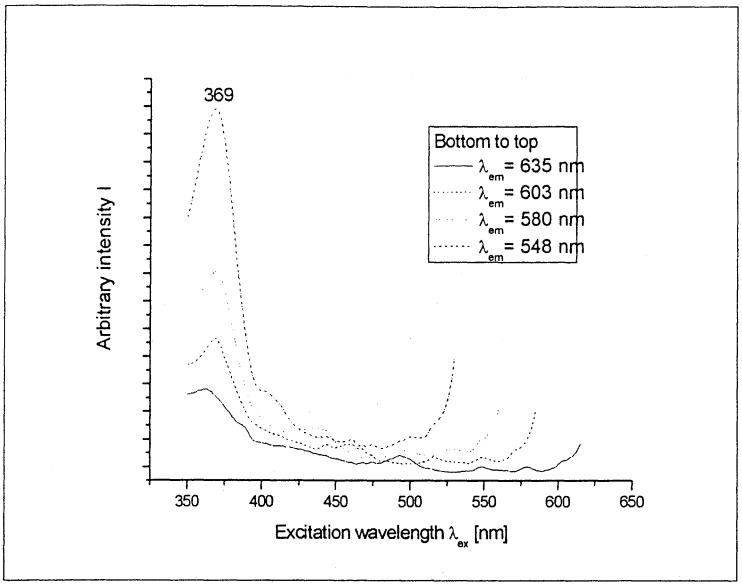

Figure 5.14: A sharp peak excitation structure is found around $\lambda_{ex} = 370\,nm$ for different long emission wavelengths beyond the peaks region

the curves in Figure 5.5 and compare them with the total intensity from the excitation $\lambda_{em} = 396\,nm + \lambda_{em} = 425\,nm$ in Figures 5.9 and 5.12. The result can be seen in Figure 5.15 where it is clear that in the region around 320-330 nm the integrated emission intensity is considerably higher than the emission from the two main peaks. This supports the idea of having a second luminescent active site in the crystal. Even though the effect is expected to be distinguishable only at cryogenic temperatures, there is enough data from the experiments that indicate that there is a second luminescent site of the cerium ions in the crystal and its effect is observable at room temperature.

Shifting to helium temperature in the excitation experiments required some previous tests since the exciting light source consisted this time on UV laser radiation. A preliminary profile with a limited excitation range was obtained at room temperature scanning the dye laser in the 357.5-363.0 nm interval but did not provide much information on the luminescent transitions in the ions given the limited range used. A new scan going from 357.5 to 378.5 nm was taken and this spectra, shown in Figure 5.16, helped to acknowledge some technical differences with the previous measurements. It was in general agreement with the expected decaying behavior taken from the same region and in particular it showed the importance of keeping the right track of changes in the background signal since unnoticed variations might lead to the discrepancies between the two sets of measured values pictured in the graph. Some of the mismatch may also be the result of measuring the intensity of total fluorescence with larger than 396 nm wavelengths[6] in this experiment in comparison with measuring only the intensity around the 396 nm emission in the former

[6]The experimental setup used a filter to block shorter than $\sim$ 400 nm wavelengths to cut-off the contribution of the scattered excitation light.

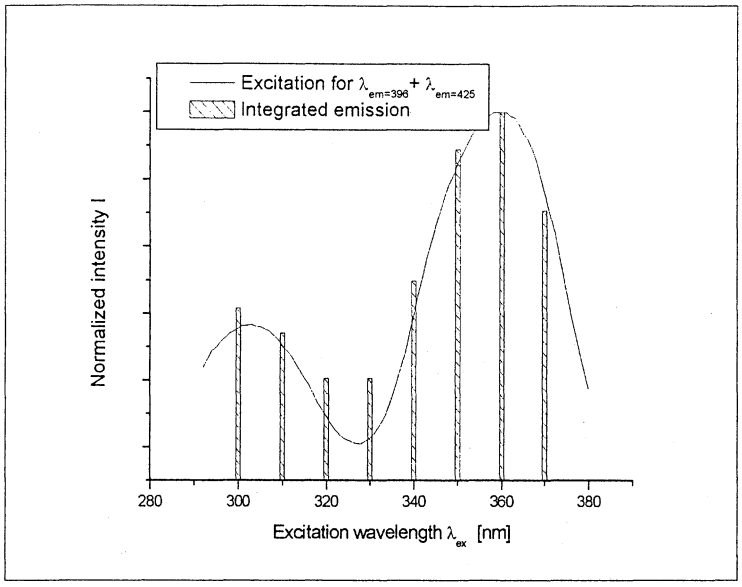

Figure 5.15: The (normalized) integrated intensity of fluorescence produced with different excitations is compared with the sum of the intensities coming from the two peaks when excited in the 290-380 nm interval. The intensities do not match only in the 320-330 nm region which suggest a contribution from a different luminescent source.

experiment plotted in Figure 5.9.

When the crystal was cooled down to $\sim$ 4K the excitation was scanned again but this time using a slightly wider range restricted only by the laser operational limits. The spectra recorded was again in general agreement with the room temperature experiments as shown in Figure 5.17. Since the reference plot was obtained with different equipment the intensities are normalized in order to make comparisons between them. For instance, it can be seen then that there is a slight narrowing in the excitation linewidth and a shift in the excitation peak to longer wavelengths. This was in agreement with the results found in literature although more significant changes in the linewidth were expected (and desired). If the deviations related to the experimental procedure are minimum then the behavior of the spectrum implies that the inhomogeneous broadening of the ions in the crystal is large even if the transitions involving phonons are minimized by the decrease in temperature. Since the phonon density per states is decreased with temperature, the mean phonon state approaches the zero phonon level and there are less fluctuations around this value. Then according to the model used (Figure 5.3) the chances for 4f-5d zero phonon transitions were expected to increase if there is an overlap between the zero phonon levels in both electronic states.

Analyzing the data in Figure 5.17 a decay in transmission was observed around $\lambda_{ex} =$ 378 nm. This information suggested that a zpl could be lying in this region and a second

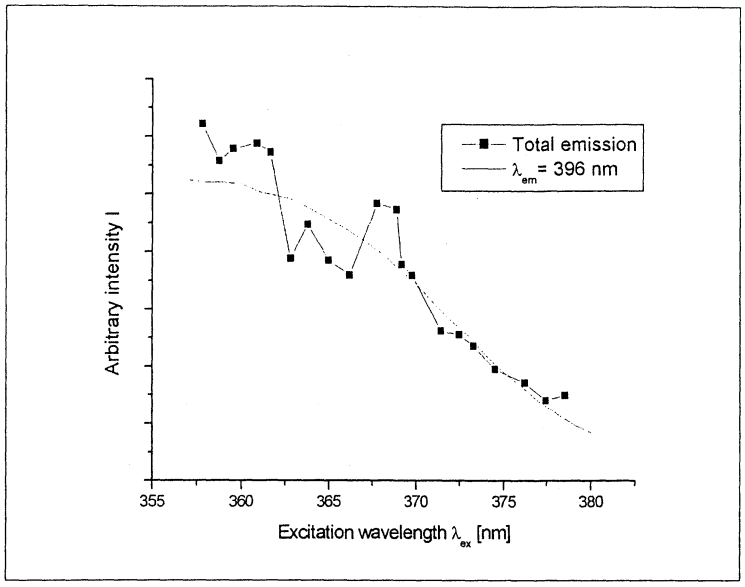

Figure 5.16: Drifts in the frequency and changes in the output power of the laser might cause the fluctuation of the signal compared to the one obtained with the spectrograph.

scan of the laser wavelength was carried out to look it. Since the zpl is expected to be narrow the chances for precisely match it with the laser wavelength might be low. In order to increase the chances, some considerations were needed in order to set limits for the laser tuning. In the proposed model for the cerium ions in the crystal (see Figure 5.13) it was assumed that the separation between phonon states in the ground and excited electronic states was the same. The Stokes shift was also determined before and with these two criteria the zpl was expected to be seen as a sharp pit in the transmission spectrum around the half value of the Stokes shift, i.e. around the 378 nm excitation wavelength. Accordingly the crystal was excited with light in the 370.5-378.2 nm interval and the spectrum obtained is shown in Figure 5.18.

The expected features of the spectrum were not observed and the indication of possible zpl for the transition was not found. There are a couple of things that might explain this result. One is that, as it was said before, the width of the peak could be very narrow and the precise wavelength could have been missed during the scan. Also, as it was shown in Figure 5.17, the inhomogeneous linewidth seems to narrow slightly but not considerably as to expect many zpl transitions from the ensemble specific excitation wavelengths. Another factor comes from experimental errors such as problems with the cooling system, laser drift and UV power fluctuations. When considered together with the signal to noise relation observed in Figure 5.8 one may suspect that small signal changes are not easily detectable. This might explain why there are not visible zpl peaks in the emission spectrum at liquid helium temperature.

Finally, the last experiment analyzed deals with the lifetime of the excited state, pre-

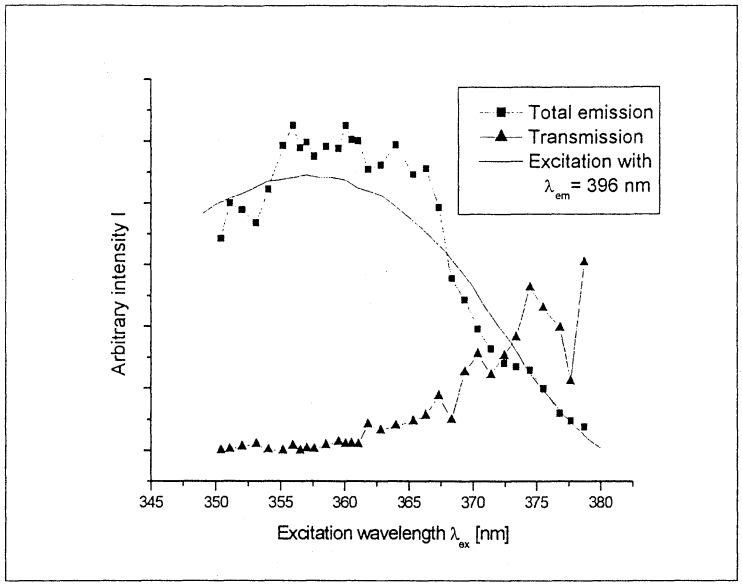

Figure 5.17: At liquid helium temperature the excitation profile seems to narrow but without sharpening as to get rid of the inhomogeneous broadening. The sudden drop in transmission might be due to a zpl being excited.

sumably the mean phonon state in the lowest level electronic level in the 5d manifold. The results of the measurements taken at liquid helium temperature are shown in Figure 5.19.

The figure shows a exponential decay fit for the experimental values. This curve serves to determine to what extent the device used (the oscilloscope mainly) to measure the decay limits the accuracy of the time decay measurements. The sooner the curve has a non-linear behavior, the sooner the measurements reveal the fluorescent states lifetime. However, once the reliability of the measurements is observed, the only interesting points are those corresponding to low resistance values. From different measurements at 50 and 100 Ω it was found that the fluorescent states have a lifetime of approximately 46 ns, a magnitude comparable to the $\sim$40 ns value reported previously in [11].

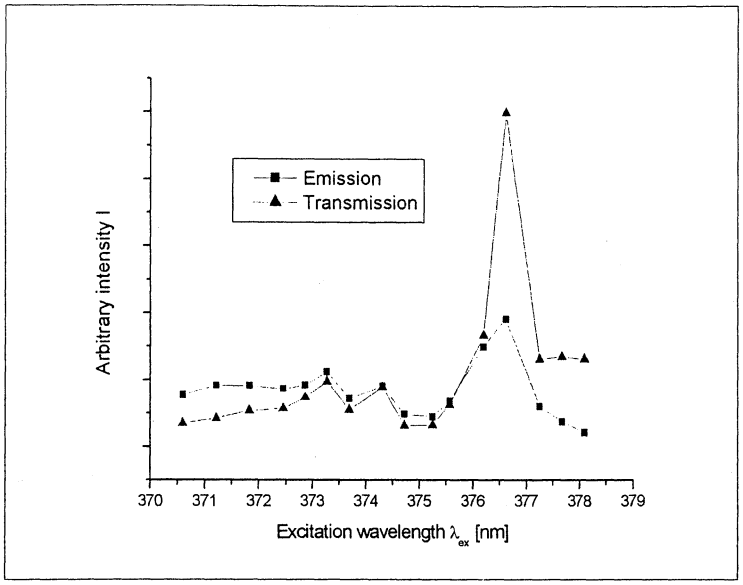

Figure 5.18: The drop in transmission is not found again in the region seen in Figure 5.17 and no zpl can be identified. $\lambda_{ex} = 320\,\text{nm}$

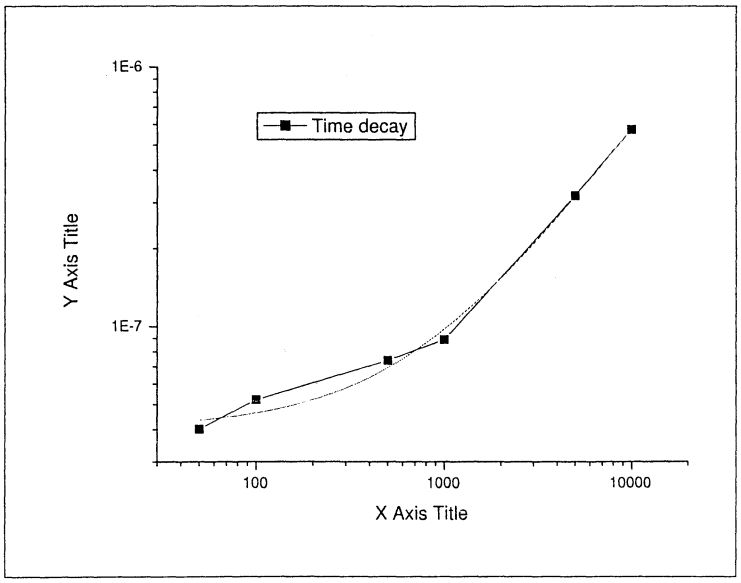

Figure 5.19: The discharge times found for different values in the resistance show an exponential decay. The mismatch with the linear decay indicates a difference between the characteristic times of the devices used and the actual decay time of the excited ions.

Chapter 6

Conclusions

Quantum computation is expected to provide an alternative to solve some of the inherent problems and limitations of current computational technology. To explore its capabilities it is required to first find an initial quantum mechanical system in which computations can be implemented. The rare-earth ions doped crystals approach for QC aims to provide such system as well as the necessary theoretical and experimental resources needed to carry out the operations. Although the approach has proven to be suitable for basic computation there are still issues to be solved.

Regarding the last step of the computation, the information readout, a single ion readout scheme has been proposed to enhance the process. This thesis was part of an effort to explore its feasibility. Some of the necessary information before the actual implementation of the scheme has been gathered as was shown in the chapter Results and Analysis. In particular the data showed that the cerium ion is a good candidate to mediate the readout process because it relaxes form the fluorescent states in a time close to 46 ns. This time is much shorter (by a factor of 10^3) than the coherence time T_2 of the ions that are used as qubits in the experiments carried out so far.

Using the information acquired in the experiments an initial model for the separation between electronic levels for the cerium in the crystal was constructed. Also, after observing that the dopant ions were absorbing and emitting at different wavelengths, an estimation on the contribution to relaxation of the phonon assisted processes was made. With this information it was also possible to determine the region in which the zero phonon line needed to drive the transitions for the readout process is expected to be seen.

The project will continue in a new stage in which finding the zpl will be one of the main purposes. Hopefully the work done during the last months will be of some use and shall provide a guide on what to do and what not. Also, by the time this thesis research ended there where some interesting insights that might help to define the path to be followed when attempting to find such and other features in the Ce^{3+}:Y_2SiO_5 crystal. In particular the validity of the Born-Oppenheimer approximation should be considered carefully when using the electronic model constructed for the ions in the crystal.

Finally, the equipment needed to carry out the upcoming experiments has been set to work properly within the requirements of the project. The different experimental problems encountered along the way were highly time-consuming and perhaps also a reason for the limitations in the results found. Fortunately the cryostat has been fixed in the weeks following after the last measurements were performed and the frequency doubler system for the dye laser was tested and characterized within this project and is now ready to use. Although it is quite likely that there will be more unexpected malfunctions in the future, the necessary devices to start over are ready.

Acknowledgements

After the long days and nights of the last six months, I have finally concluded this project. I enjoyed and learned so much doing it and maybe someone will read it and find it useful. Or maybe not. Anyway, I want to thank all the people who either directly or indirectly were involved with this project.

First I want to thank my supervisor Stefan Kröll for giving me the opportunity to come to Lund and work on my Master's thesis in his group, for his advice and his patience. I want to thank also to the entire Photon Echo Group for their constant support and camaraderie. Particularly I want to thank Brian Julsgaard for sharing his knowledge with me and for all the guidance throughout the project. I want to thank Lars Rippe for many things: the discussions, the jokes, the advices, the housing but most of all for his friendship. Thanks to Andreas Walther for helping me out whenever I got questions in the lab and on the board and for being such a cool officemate. Thanks and good luck to Atia, Magnus and Johan. Also I want to thank the entire Atomic Physics Division at LTH for receiving me during these months, in particular to Anders Persson for helping me fighting the laser. Additionally I want to thank specially to Mikael Fogelström in Chalmers University of Technology for reviewing my thesis.

I want to thank all my family, all of them, for being so close even when we are so far away. Thanks to my mother for all her love, support and wise advice. Thanks to my father for showing me that things can change for good. Thanks to my brothers, my sister and my other set of parents for being there. Thanks to my old friends for their support and love over the years. Thanks to the new ones for coming in the right time. Thanks to all those who made my stay in Sweden pleasant, interesting and unforgettable.

Finally I want to thank the STINT Foundation in Sweden and the Secretaría de Educaci'on Publica in México for their economic support that helped to make this possible.

Bibliography

[1] L. K. Grover. Quantum mechanics helps in searching for a needle in a haystack. *Phys. Rev. Lett.*, 79:325, 1997.

[2] P. W. Shor. Polynomial time algorithms for prime factorization and discrete logariths on a quantum computer. *SIAM J. Comput.*, 26:1484, 1997.

[3] J. J. Sakurai. *Modern Quantum Mechanics.* Addison Wesley, 1994.

[4] P. W. Milonni and J. H. Eberly. *Lasers.* John Wiley & Sons, New York, 1988.

[5] M. A. Nielsen and I. L. Chuang. *Quantum Computation and Quantum Information.* Cambridge University Press, 2000.

[6] D. P. DiVincenzo. The physical implementation of quantum computation. *arXiv:quant-ph/0002077v3.*

[7] M. Nilsson. *Coherent interactions in rare-earth-ion doped crystals for applications in quantum information science.* Doctoral Thesis, Lund Institue of Technology, Lund, Sweden, 2004.

[8] B. H. Bransden and C. J. Joachain. *Physics of atoms and molecules.* Longman, Essex, UK, 1996.

[9] I. Roos and K. Mølmer. Quantumquantum computing with composite pulses and coherent population trapping. *Phys. Rev. A*, 69:022321, 2004.

[10] B. Henderson and G. F. Imbusch. *Optical spectroscopy of inorganic Solids.* Oxford University Press, New York, 1989.

[11] M. Lastusaari J. Legendziewicz J. Niittykoski F. Pellé T. Aitasalo, J. Hölsa. Delayed liminescence of ce^{3+} doped y_2sio_5. *Opt. Mat.*, 26:107–112, 2004.

[12] S. Tian H. Jiao, F. Liao and X. Jing. Influence of rare earth sc and la to luminescent properties of fed blue phosphor y_2sio_5:ce. *J. Electrochem. Soc.*, 151:J39–J42, 2004.

[13] M. J. Weber. Optical spectra of ce^{3+} and ce^{3+}-sensitized fluorescence in yal_3. *J. Appl. Phys.*, 44:3205–3208, 1973.

[14] C. L. Melcher J. S. H. Suzuki, T. A. Tombrello and Schweitzer. Uv and gamma-ray excited luminescence of cerium-doped rare-earth oxyorthosilicates. *Nucl. Instr. & Meth*, A320:263–292, 1992.